

Taylor & Francis
Taylor & Francis Group

Journal of Asian Architecture and Building Engineering

ISSN: 1346-7581 (Print) 1347-2852 (Online) Journal homepage: www.tandfonline.com/journals/tabe20

Seismic resilience of existing RC dual-system buildings during the 2023 Kahramanmaraş earthquakes: a case study

Zeliha Tonyali, Adnan Kiral, Mustafa Ergun & Reyes Garcia

To cite this article: Zeliha Tonyali, Adnan Kiral, Mustafa Ergun & Reyes Garcia (26 Sep 2025): Seismic resilience of existing RC dual-system buildings during the 2023 Kahramanmaraş earthquakes: a case study, Journal of Asian Architecture and Building Engineering, DOI: 10.1080/13467581.2025.2564110

To link to this article: https://doi.org/10.1080/13467581.2025.2564110

© 2025 The Author(s). Published by Informa UK Limited, trading as Taylor & Francis Group on behalf of the Architectural Institute of Japan, Architectural Institute of Korea and Architectural Society of China.

Published online: 26 Sep 2025.

Submit your article to this journal

View related articles

View Crossmark data

Full Terms & Conditions of access and use can be found at
https://www.tandfonline.com/action/journalInformation?journalCode=tabe20

JOURNAL OF ASIAN ARCHITECTURE AND BUILDING ENGINEERING
https://doi.org/10.1080/13467581.2025.2564110

Taylor & Francis
Taylor & Francis Group

BUILDING STRUCTURES AND MATERIALS

OPEN ACCESS Check for updates

Seismic resilience of existing RC dual-system buildings during the 2023 Kahramanmaraş earthquakes: a case study

Zeliha Tonyali[a], Adnan Kiral[a], Mustafa Ergun[b] and Reyes Garcia[c]

[a]Department of Civil Engineering, Faculty of Engineering and Architecture, Recep Tayyip Erdogan University, Rize, Türkiye; [b]Department of Civil Engineering, Bayburt University, Bayburt, Türkiye; [c]Built Environment & Sustainability Research Cluster, School of Engineering, The University of Warwick, Coventry, UK

ABSTRACT

This study investigates the seismic resilience of an existing reinforced concrete (RC) dual-system during the 2023 Kahramanmaraş earthquakes. The shear wall-frame dual building was designed according to the Turkish guidelines (TEC 2007) and experienced negligible damage during the earthquakes, whereas all neighboring buildings collapsed. The case study building is modeled in SAP2000® adopting a lumped plasticity approach. The 3D building model was subsequently subjected to pushover and nonlinear time-history analyses (NTHAs) using real ground motions recorded during the first and strongest mainshock of the Kahramanmaraş earthquakes ($M_w = 7.7$ Pazarcik earthquake). The results from the NTHAs indicate that the maximum inter-story drift (IDR) ratios on all floors of the case study building remained below the Immediate Occupancy performance level (IDR = 1.0%). Moreover, the dual-system building designed with TEC 2007 survived the earthquakes without damage, even when the design earthquake scenarios exceeded those considered in the new and more stringent TBEC 2018 (i.e. a 475 return period). The limited damage experienced by the RC dual-system building can be largely attributed to its high wall index ($WI = 1.5\%$ and 1.84%) and high average lateral stiffness index ($H/T \geq 45.3$), which are above the minimum values ($\rho = 0.6\%$ and $H/T \geq 45$) suggested in previous research. This study also highlights the critical importance of site-specific ground motion selection, particularly in the context of Hatay province, where the seismic demands exhibited significant variability and intensity. This study contributes to a better understanding of the resilience of RC shear wall-frame buildings in seismic zones.

ARTICLE HISTORY
Received 10 April 2025
Accepted 16 September 2025

KEYWORDS
RC shear wall-frame building; 2023 Kahramanmaraş earthquakes; nonlinear time-history analyses; Inter-story drift ratio; pushover analysis

1. Introduction

In recent decades, rapid development and population growth in Türkiye led to the widespread construction of multi-story reinforced concrete (RC) buildings. This has led to the uncontrolled and unsupervised construction of buildings, many of which are exposed to high levels of seismic hazard. Moreover, a large proportion of existing buildings were built before the introduction of modern seismic codes, thus making them highly vulnerable to earthquakes.

The Kahramanmaraş earthquakes on 6 February 2023, produced extensive damage and collapse of thousands of RC buildings across Türkiye and Syria. Previous studies have examined the effects of these earthquakes on RC buildings (Ince 2024; Ivanov and Chow 2023; Mertol et al. 2023; Ozturk, Arslan, and Korkmaz 2023; Sezgin et al. 2024; Turan et al. 2024), industrial facilities (Sagbas et al. 2024), masonry structures (Erkek and Yetkin 2023; Işık et al. 2023; Onat et al. 2023), cross-laminated timber buildings (Tonyali, Alemdağ, and Kibar 2024), school buildings (Ozturk et al. 2023), bridges (Bas et al. 2024) and water tanks (Mardani, Şahin, and Kaya 2024; Onder Cetin et al. 2024; Toprak et al. 2025). Past studies (Askan et al. 2025; Ibrahim, Makhloof, and Ren 2024; Kazaz, Avşar, and Dilsiz 2024; Kıral and Gürbüz 2024; Ozdemir 2024; Tonyali and Kiral 2024; Vuran et al. 2025) have also investigated the seismological characteristics of the Kahramanmaraş earthquake sequence and its effect on the seismic performance of buildings. For instance, Vuran et al. (Vuran et al. 2025) analyzed the structural collapse of pre-2000 and post-2000 RC buildings during such earthquakes. They found that many post-2000 RC buildings have experienced extensive structural damage and tilting. Vuran et al. suggested revising the response spectrum in the Turkish code, primarily because the DD-1 (2% probability of exceedance in 50 years) seismic hazard level was exceeded for long-period structures. Lashgari et al. (Lashgari et al. 2024) studied the local site effects in Kahramanmaraş province and found that damage was mostly concentrated on 8- to 10-story buildings situated on alluvial soils. Likewise, Lashgari et al. also concluded

CONTACT Adnan Kiral adnan.kiral@erdogan.edu.tr Department of Civil Engineering, Faculty of Engineering and Architecture, Recep Tayyip Erdogan University, Rize, Türkiye; Reyes Garcia reyes.garcia@warwick.ac.uk School of Engineering, University of Warwick, Library Road, Coventry CV4 7AL, UK

© 2025 The Author(s). Published by Informa UK Limited, trading as Taylor & Francis Group on behalf of the Architectural Institute of Japan, Architectural Institute of Korea and Architectural Society of China.
This is an Open Access article distributed under the terms of the Creative Commons Attribution License (http://creativecommons.org/licenses/by/4.0/), which permits unrestricted use, distribution, and reproduction in any medium, provided the original work is properly cited. The terms on which this article has been published allow the posting of the Accepted Manuscript in a repository by the author(s) or with their consent.

that 10-story buildings could resist spectral accelerations of up to 0.85 g, which is approximately 1.8 times higher than the design limits recommended by the previous TEC 2007 (2007) seismic code.

Past studies have found that many buildings in Türkiye do not comply with earthquake code requirements, thus increasing their vulnerability. Mertol et al. (Mertol et al. 2023) investigated the damage patterns of collapsed and severely/moderately damaged buildings built between 1975 and 2000. Structural deficiencies included short development lengths of bars, inadequate bents of stirrup ends, use of poor-quality materials, weak column-strong beam strength hierarchies, and a lack of proper inspection during construction. Demir et al. (Demir et al. 2021) concluded that numerous failures are due to use of poor quality concrete, inadequate detailing, and deficiencies in the design and construction of the project, based on their field observations following the 2020 Elazığ earthquake (M_w 6.8). Ince (Ince 2024) studied how well current Turkish regulations were followed in design; they identified key design and construction issues that led to RC building failures in Adıyaman province. Pujol et al. (Pujol et al. 2024) surveyed around 250 RC buildings ranging from 2 to 16 stories in the area extending from Antakya to Malatya. They concluded that a strong correlation exists between the extent of observed damage and the Wall Index (*WI*) and Column Index (*CI*), defined as the ratio of cross-sectional area to total floor area. Over 90% of the surveyed buildings with $WI < 0.1\%$ experienced severe damage. Notably, around 96% of critically damaged buildings, deemed too vulnerable to withstand aftershocks, also had a $WI < 0.1\%$. Pujol et al. underlined the need for more stringent design guidelines that encourage the construction of structures that either comply with or exceed *WI* and *CI* criteria in Türkiye and other seismically active regions. Yön et al. (Yön et al. 2024) examined the magnitude of earthquakes and the structural deficiencies in buildings. It was found that the observed design flaws in the collapsed structures were similar to those observed in previous earthquakes.

More recently, Atmaca et al. (Atmaca et al. 2025) analysed the collapse of 400 RC buildings in the affected region following the 2023 Kahramanmaraş earthquakes. A major cause of collapses was attributed to noncompliance with the building code at the time of construction, including construction-phase errors (43.58% of cases), mistakes in structural analysis (25.57%), licensing issues (24.77%), and post-construction factors (6.07%). Atmaca et al. also highlighted the importance of adopting the latest codes in design, as well as better inspections, and use of better-quality materials to improve earthquake resilience. Altunişik et al. (Altunişik et al. 2023) investigated the structural deficiencies of RC buildings affected by the devastating 2023 Kahramanmaraş earthquakes. Based on field observations, Altunişik et al. identified two main sources of damage: design-stage issues (e.g. weak columns, soft stories, short columns, and poor detailing), and construction-stage problems (including low-quality concrete, improper reinforcement placement, and poor workmanship). To support these findings, Altunişik et al. also conducted a nonlinear finite element analysis of a collapsed RC building. The numerical results confirmed the causes of failure observed in the field, thus highlighting the high vulnerability of the current building stock in Türkiye.

The widespread damage caused by the Kahramanmaraş earthquakes on relatively new buildings designed with TEC 2007 (T2007) or TBEC 2018 (2018) highlighted that, despite progress, a lack of understanding of seismic design philosophy and poor quality control during construction can still lead to high losses (Kazaz, Avşar, and Dilsiz 2024). However, whilst numerous RC buildings performed very well during the Kahramanmaraş earthquakes, little research has examined their behavior so that good practices can be identified and replicated. For instance, many RC dual-system buildings (shear wall-frame) in Kahramanmaraş province experienced minor or negligible damage during the earthquakes. In dual-system buildings, the shear walls are specifically designed to resist lateral forces. The high stiffness and strength of shear walls effectively control lateral drifts (thus minimizing damage), whereas frames mostly carry vertical loads. Previous studies (e.g Er 2025; Kap 2025; Lagos et al. 2012; Ozkul et al. 2019; Xu et al. 2023) have investigated the effectiveness of these systems at reducing earthquake-related damage. For example, Sonmez et al. (Sonmez et al. 2025) surveyed the performance of 242 RC buildings during the 2023 Kahramanmaraş earthquakes. They mainly focused on low- and mid-rise RC moment frames, hybrid frame-wall systems, and RC wall buildings. Whilst RC frames and hybrid systems generally experienced significant damage due to design deficiencies and high drift demands, RC wall buildings performed well if enough structural walls were present. Both field observations and fragility analyses confirmed that properly designed RC wall systems offer better seismic safety compared to frame-based systems. Similar observations were made by Kazaz (Kazaz 2025), who indicated that RC wall buildings with sufficient wall indices survived the Kahramanmaraş earthquakes. While much research has focused on investigating the behavior of deficient RC buildings during the earthquakes, to date, limited research has examined the seismic performance of resilient RC dual-system buildings. Successful case studies can help to better understand the vulnerability and resilience of existing buildings, which in turn can minimize the associated seismic losses in future earthquakes. Moreover, only a few studies (Akinci et al. 2025; Buckreis et al. 2024; Lashgari et al. 2024) have used real seismological records from Kahramanmaraş earthquakes to investigate their effects on structures. Recent studies (Altunişik et al. 2023; Kazaz,

Avşar, and Dilsiz 2024; Vuran et al. 2025) have also identified a lack of research on actual case study buildings to provide a further understanding of the effectiveness of Turkish codes at controlling damage.

This study investigates the seismic resilience of an existing RC dual-system building during the Kahramanmaraş earthquakes. To achieve this, a case study building designed with TEC 2007 (2007) was modeled using SAP2000® software. The shear wall-frame dual building experienced negligible damage during the earthquakes, whereas all neighboring buildings collapsed. The building was subjected to static pushover and nonlinear time-history analyses (NTHA) using real ground motions recorded during the Pazarcik earthquake ($M_w = 7.7$). The results are presented and discussed in terms of global (inter-story drifts and base shear) and local (rotations and shear strengths) behavior. The lessons learned and implications for best design/construction practices in Türkiye are also discussed. The results of this study contribute to a better understanding of the resilience of RC shear wall-frame buildings located in zones with high seismic hazard, which in turn can help promote best practices in design and construction in Türkiye and other developing countries with high seismic hazard.

2. Description and analysis of case study building

2.1. Seismic setting and local soil conditions at study site

The Kahramanmaraş earthquakes mainly affected 11 provinces of Türkiye (see Figure 1), where almost 87% of the existing structures are RC buildings (SBP 2023). The data in Figure 1 show that the buildings in Hatay province experienced the heaviest damage (251,555 structures). The investigated case study building (Rende building) is located in Antakya, the most affected district of Hatay province. Figure 2a shows the seismicity of Hatay province within Türkiye's seismic hazard map. Antakya city experiences intense seismic ground motions as it lies on a soft Holocene sediment-filled basin (Erdik et al. 2023), which amplifies ground shaking and thus increases building damage (Över et al. 2011). Figure 2b shows the location of the Rende case study building (black star) on the soil map of Antakya, along with the location of other structures that experienced damage or collapse. Most of the damage is concentrated around the Orontes (Asi) Basin, which is known to have the weakest soil in the area.

2.2. Seismic records

The seven stations closest to the case study building (S3123, S3124, S3126, S3129, S3131, S3141, and S4614) were considered in the analysis, as shown in Figure 3a-b. Five stations are within the city of Antakya, whereas the Defne and Pazarcık stations (i.e., S3129 and S4614, respectively) are outside the city, as reported in Table 1. The table also reports the average shear wave velocity (V_{s30}), soil type classification, epicentral distance R_{epi}, and the distance from the case study building to the stations. Appendix A summarizes the

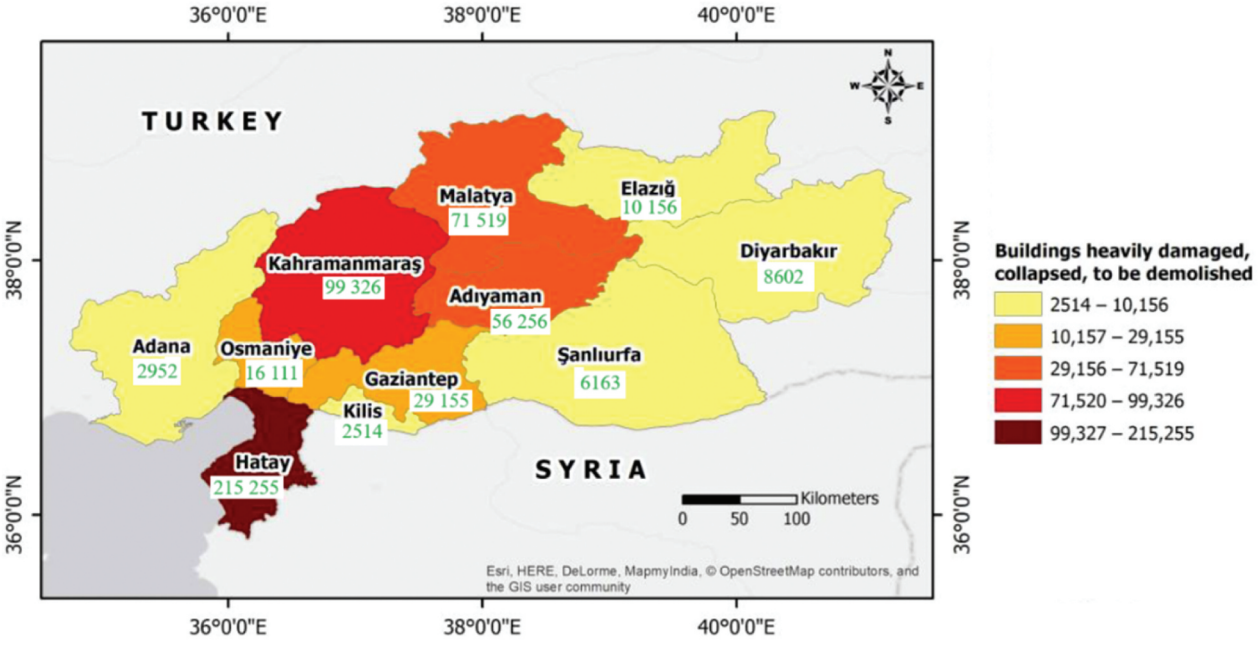

Figure 1. Provinces affected by the Kahramanmaraş earthquakes and data on building damage in these provinces (modified after (SBP 2023)).

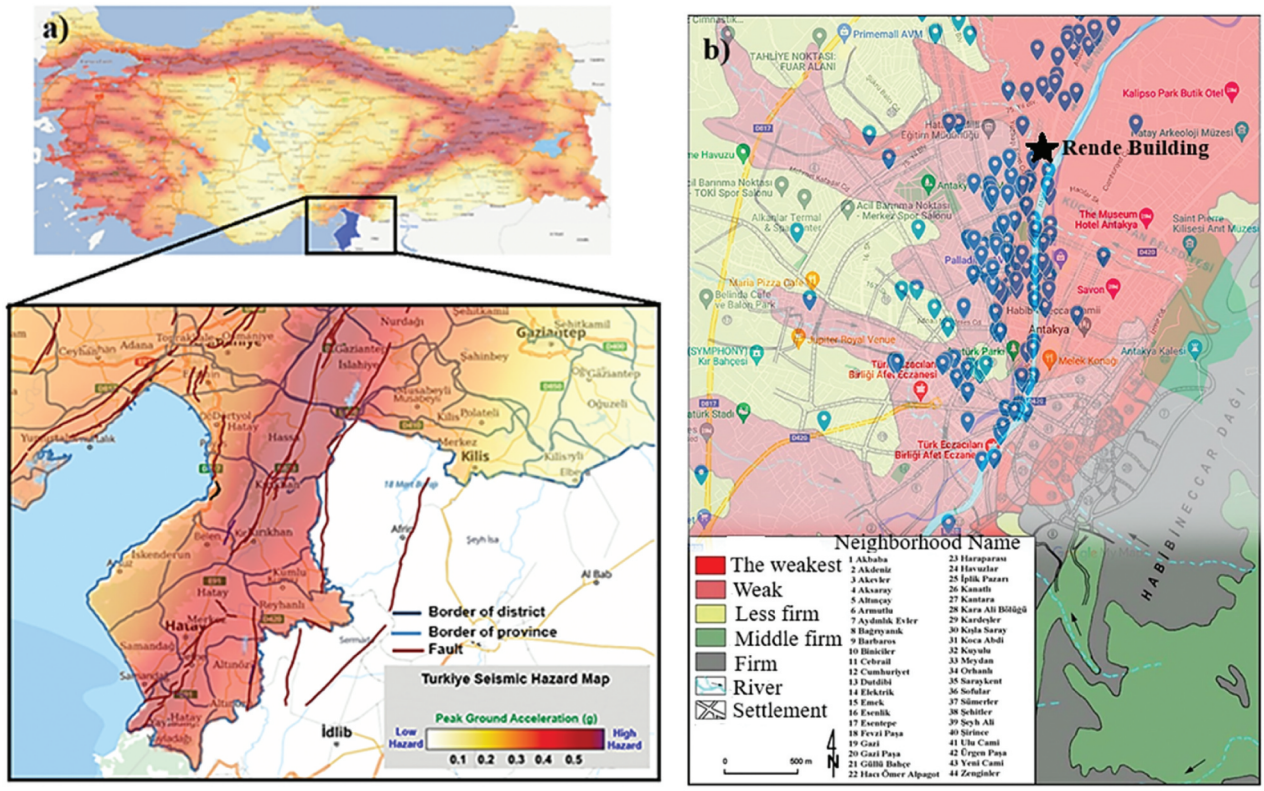

Figure 2. (a) Seismicity of Hatay in Türkiye's hazard map (modified after (AFAD 2023a)), (b) location of the Rende building and Antakya's soil properties (modified after (Büyüktopcu 0000)).

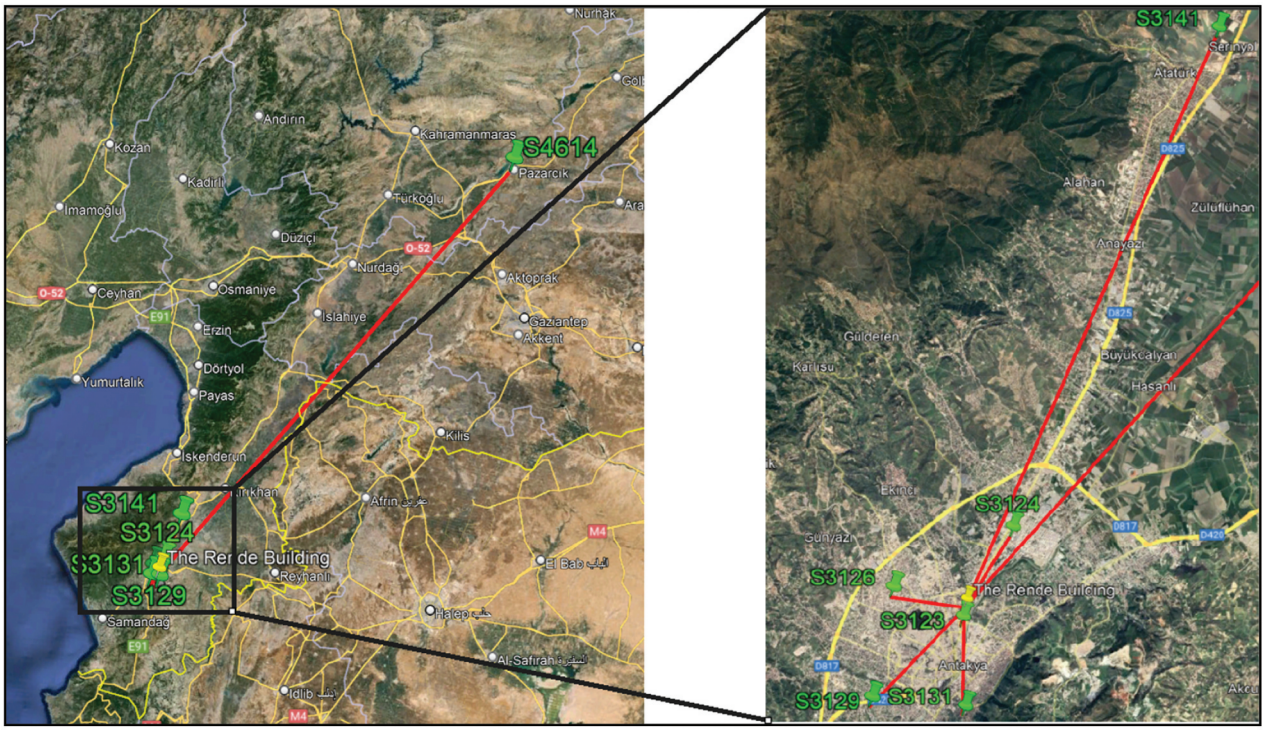

Figure 3. Selected stations in Hatay and Kahramanmaraş provinces (31xx stations are located in Hatay, whereas 46xx station is in Kahramanmaraş province).

details of the recorded ground motions, including the time histories of the acceleration, velocity, and displacement of the three components of the Pazarcik (M_w 7.7) earthquake, which was the strongest of the two Kahramanmaraş earthquakes. Note that station S4614 is closest to the epicenter of the Kahramanmaraş earthquakes; therefore, this station is expected to have the largest accelerations. Likewise, station S3123 was the

Table 1. Details of seismic stations (modified after (AFAD 2023b)).

Station ID	Location	V_{s30} (m/s)	Soil types		R_{epi} (km)	Distance to building (km)	Lat. (°)	Long. (°)
			EC8	TBEC 2018				
S3123	Antakya	469	B	C	143.00	0.57	36.21423	36.15973
S3124	Antakya	283	C	D	140.11	2.39	36.23870	36.17220
S3126	Antakya	350	C	D	143.54	2.10	36.22020	36.13750
S3129	Defne	447	B	C	146.39	3.91	36.19117	36.13430
S3131	Antakya	567	B	C	144.98	3.11	36.19121	36.16328
S3141	Antakya	338	C	D	125.42	17.80	36.37260	36.21973
S4614	Pazarcık	541	B	C	31.42	173.00	37.48513	37.29775

closest to the case study building. Table 2 lists the shear wave velocity classification (V_{s30}) for different soil types according to Eurocode 8 (2004) and TBEC 2018 (2018). The case study building was located in soil type Z2 (or ZC according to TBEC 2018). The ground motions recorded at the seven stations (Table 1) are used later to perform nonlinear time history analyses on the case study building.

Figs. 4a-g compare the horizontal response spectra and mean response spectra of the Pazarcik earthquake (M_w7.7) at selected stations. The figures include the ground motion levels DD-1, DD-2, DD-3 and DD-4 included in the TBEC 2018 code for soil type ZC. Each graph in Figures 4a-g includes multiple acceleration components, including DD-1 to DD-4, E-W (east–west component), N-S (north–south component), and geometric mean of accelerations (GeoMean). In TEC 2018, the shear wave velocities V_{s30} were 360–760 m/s and 180–360 m/s for soil types ZC and ZD, respectively, as shown in Table 2. The elastic design spectra of DD-1, DD-2, DD-3, and DD-4 were associated with return periods of 2475, 475, 72 and 43 years, respectively. Accordingly, ground motion levels DD-1 and DD-2 were deemed as the largest earthquake ground motion and the design earthquake ground motion, respectively. The maximum spectral accelerations at the considered stations were between 1.23 and 6.27g in the E-W direction and between 0.87 and 7.30g in the N-S direction. The results in Figures 4a-g show that S3126, S3129, S3141, and S4614 are above both the DD-1 and DD-2 (design spectrum) ground motion levels. Moreover, the spectral accelerations of the S4614 Pazarcik station are considerably above the design spectrum values for all earthquake ground motion levels (the maximum spectral acceleration is 6.27g for the E-W direction, and 7.30g for the N-S direction). Although the largest spectral accelerations are at S4614 Pazarcik station for short periods, spectral acceleration values are higher for periods longer than 0.5 s for stations S3123, S3124, and S3129.

2.3. Details of case study RC building

The Rende building is a residential structure built in 2012 following the TEC 2007 code. Figure 5a shows the location and general view of the building (from Google Street) before the Kahramanmaraş earthquakes. Figure 5a shows that the building was surrounded by several buildings of similar heights and materials. The aerial view in Figure 5b shows that after the earthquakes, the case study building survived, whereas the rest of the neighboring buildings collapsed. Figure 6 shows the floor plan of the building as provided by the designers, including the dimensions of the RC shear walls (SW), columns (C), and beams (B). The case study building is symmetric about one axis (axis 6) and approximately regular in plan, as shown in Figure 6. The structural system of the building consisted of only six columns, with the remaining vertical load-bearing elements composed entirely of shear walls. Accordingly, the main lateral resistance system consisted of shear wall frames. The building has one basement floor and five floors above it (B1F and 5F). The building was constructed on a raft foundation with a 90 cm encasement width and a 60 cm foundation depth. The thickness of the slabs was 12 cm, except for the balconies where the slabs were 15 cm thick. The height of the basement floor was 3.0 m, whereas the height of the other floors was 2.9 m. Accordingly, and the total building height was 20.6 m. The dead and live loads used in the original design were 3.96 kN/m^2 and 1.77 kN/m^2, respectively. A post-earthquake survey after the Kahramanmaraş earthquakes revealed that the case study building experienced negligible damage.

Table 2. Soil classification in TBEC 2018 (2018), Eurocode 8 (2004) and study site.

TBEC 2018		Eurocode 8		Rende building
Soil class	V_{s30} (m/s)	Soil class	V_{s30} (m/s)	V_{s30} (m/s)
ZA	> 1500	A	> 800	Z2 (TEC 2007)
ZB	760 – 1500	B	360 – 800	400–700 m/s
ZC	360 – 760	C	180 – 360	
ZD	180 – 360	D	< 180	
ZE	< 180			

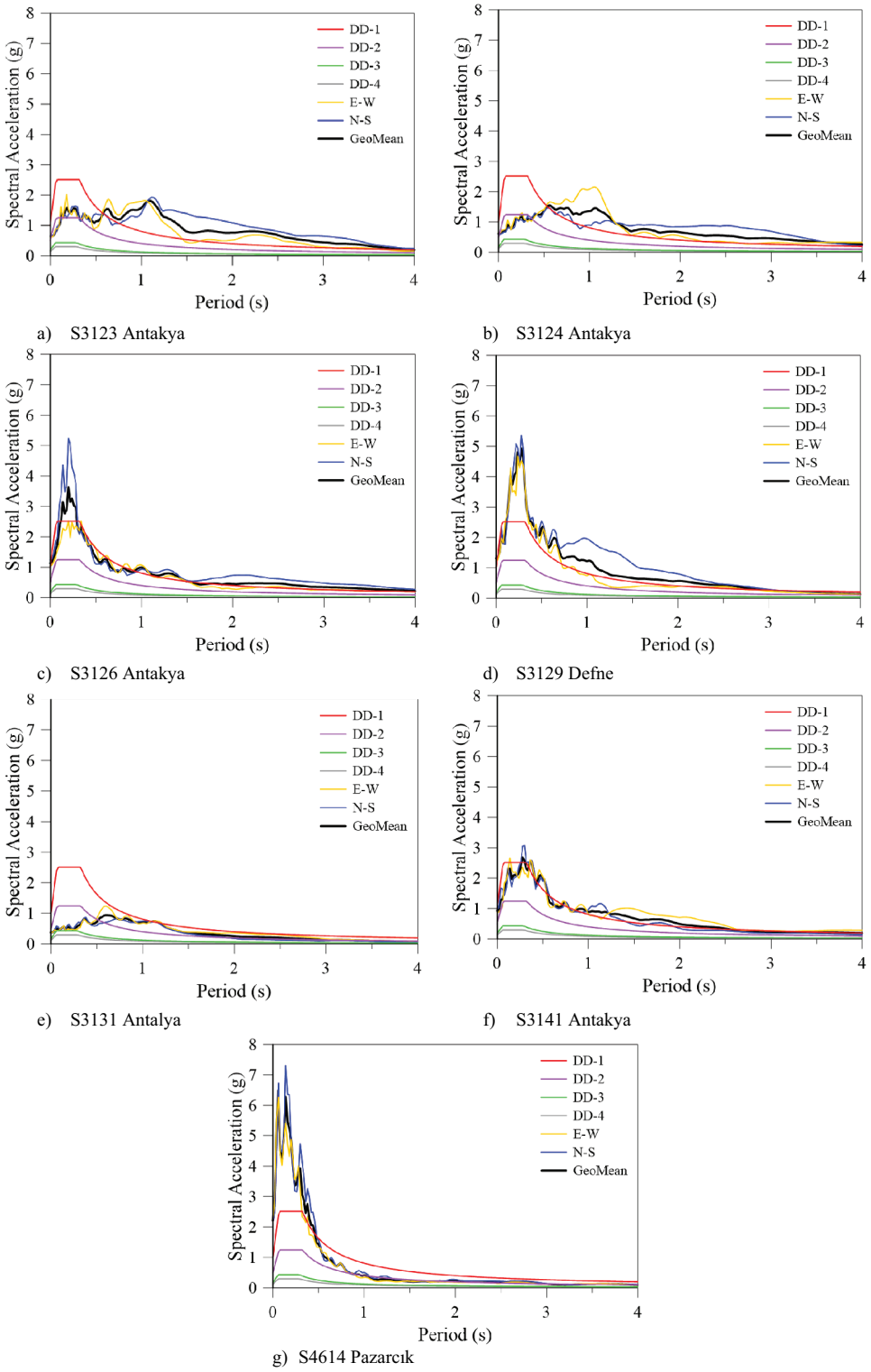

Figure 4. (a)-(g) Horizontal response spectra (5% damping) and design spectra in TBEC 2018 (2018) at selected stations due to Pazarcik (M_w 7.7), earthquake (data sourced from (AFAD 2023a)).

Indeed, only a crack was observed at the intersection of beam BG09 and the subjacent wall (see Figure 7).

2.4. Modeling approach in SAP2000®

The case study building was modeled in 3D using SAP2000® v24 software (CSI 2024). Previous studies have shown that this software is suitable for nonlinear analysis of RC structures (Inel, Cayci, and Meral 2018; Prince et al. 2023). The columns and beams were modeled using frame elements, whereas the slabs and shear walls were modeled using area elements. Figures 8a-c show typical examples of the discretization of the concrete and steel reinforcement in the beams (Figure 8a), columns (Figure 8b) and walls (Figure 8c). The material properties of the building were obtained from the

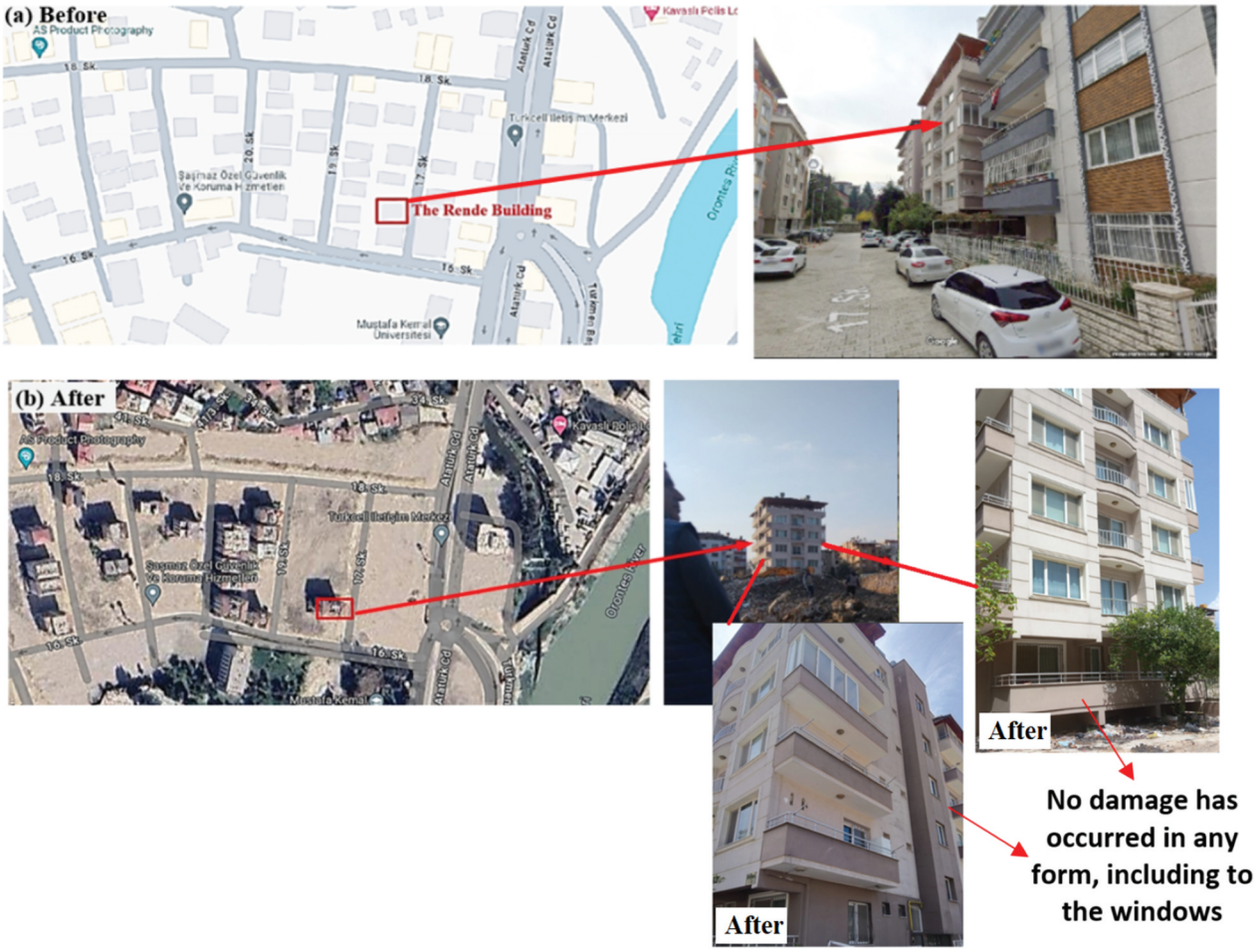

Figure 5. Case study Rende building (a) before and (b) after Kahramanmaraş earthquakes.

records provided by the designer. According to these data, the yield and ultimate strength of the steel reinforcement were $f_y = 413$ MPa and $f_u = 620$ MPa, respectively, and the concrete compressive strength and modulus of elasticity were $f_c = 25$ MPa and $E_c = 30\ 250$ MPa, respectively. Table 3 summarizes the section properties as well as the reinforcement steel and concrete properties adopted in the modeling. The soil properties and seismic parameters (obtained from AFAD (AFAD 2023a)) for the case study site are listed in the table. Based on the structural model, the total weight of the building was determined to be approximately 1271 t.

The material nonlinearity of concrete and reinforcing steel was explicitly considered in the modeling. For confined concrete, a nonlinear stress-strain relationship was defined adopting Mander et al.'s model (Garcia, Hajirasouliha, and Pilakoutas 2010; Mander, Priestley, and Park 1988). Likewise, unconfined concrete was modeled using a parabolic-linear curve in accordance with ASCE 41–17 (2017). The steel material was modeled using a bilinear elastoplastic stress-strain relationship with strain hardening. These material models were used in SAP2000®'s section designer to perform moment-curvature analyses for each member cross-section. The resulting curves were employed to define the nonlinear hinge properties automatically, ensuring that the element behavior reflected realistic material response under cyclic loading. By applying the modified Takeda hysteresis model (bilinear factor $r = 0.05$, $\alpha = 0.4$ and $\beta = 0.2$), both material and geometric nonlinearities were effectively captured in the nonlinear time-history analysis. This dual-level nonlinear modeling (material and element hysteresis) ensured an accurate simulation of the seismic response of the case study building.

It should be noted that the use of nominal design values for both concrete and steel reinforcement in the analysis may introduce certain uncertainties in the results. Nevertheless, these values are derived from established design standards, which are intended to provide conservative estimates of material properties. Although direct material testing could not be conducted, this approach is consistent with standard practices in structural assessment studies. Furthermore, to better capture the energy dissipation and ensure realistic structural behavior, approximate mean strength values for the constituent materials (i.e. steel and concrete) were adopted, following the modelling strategies employed in previous studies (e.g (Car, Oller, and Oñate 2000; Jin et al. 2025; Vielma, Barbat, and Oller 2010).

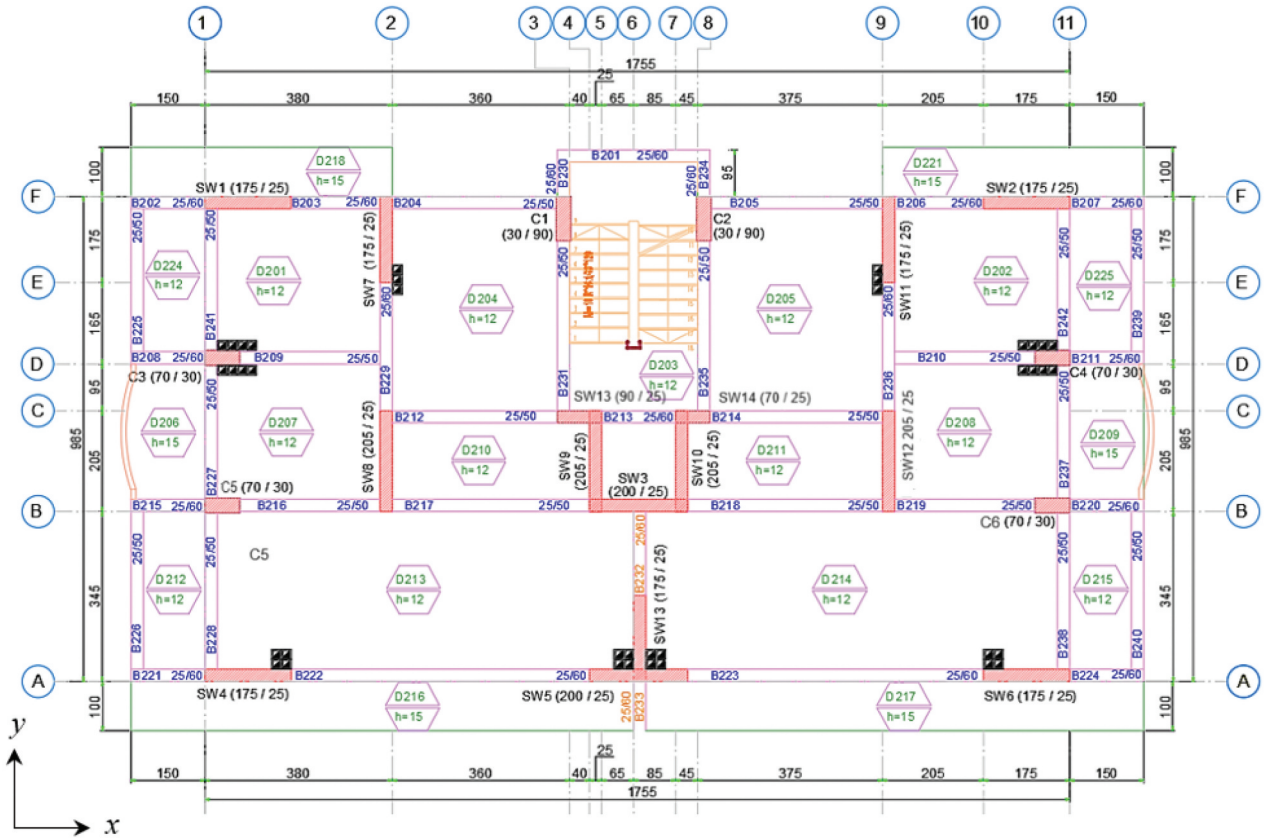

Figure 6. Floor plan of case study building (units: cm).



Figure 7. Negligible damage under beam BG09 after Kahramanmaraş earthquakes.

It should also be noted that whilst the case study building had some masonry infill walls, these were not explicitly modeled. This is because a gap existed between the columns/walls of the building and the infill walls, and therefore the latter did not contribute to resist seismic load. This was confirmed by field observations as all infill walls were undamaged after the Kahramanmaraş earthquakes occurred. However, this modeling approach should not be extended to other buildings where stiff infill walls connected to columns/walls can significantly increase the lateral stiffness of a building and reduce its fundamental period.

2.5. Plastic hinges and soil–structure interaction

A lumped plasticity approach was adopted for the RC frame elements. Accordingly, plastic hinges were explicitly assigned at both ends of beams and columns. For beams, M3 moment hinges were defined as *Auto ASCE41–17–M3*, which automatically generates standardized moment-rotation backbone curves in accordance with ASCE 41–17 (2017) guidelines. These curves incorporate strength and stiffness degradation based on a bilinear (kinematic) hysteretic model governed by the modified Takeda rule, which accounts for cyclic degradation effects. Likewise, P-M2-M3 plastic hinges

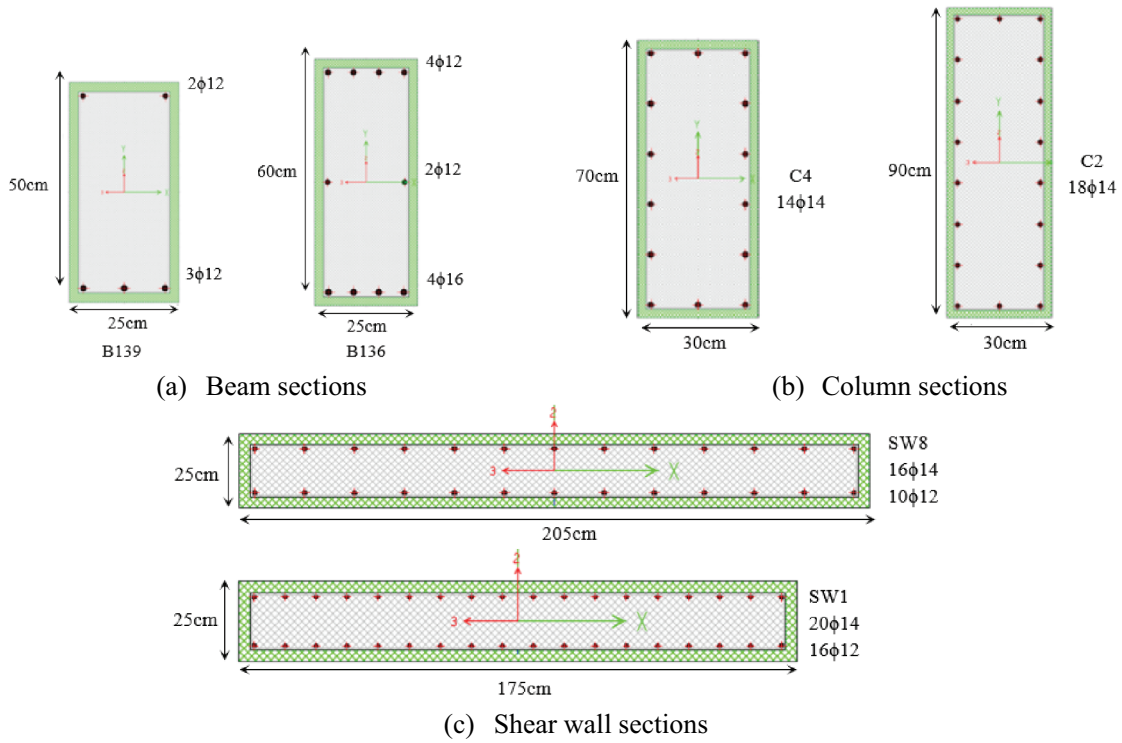

Figure 8. Typical discretization of concrete and steel reinforcement in (a) beams and (b) columns adopted in SAP2000®.

Table 3. Modeling details adopted for case study building.

Reinforcement details	Column	Beam	Shear wall
Dimension of section (cm^2)	30 × 70 30 × 90	25 × 50 25 × 60	175 × 25 200 × 25 205 × 25
Reinforcement bar diameter range (mm)	ϕ14 - ϕ18	ϕ12- ϕ16	ϕ12- ϕ16
Confinement bar size (mm)	ϕ8	ϕ8	ϕ8
Confinement bar area (mm^2)	50.3	50.3	50.3
Bar cover (mm)	25	15	25
Material properties			
Concrete grade	C25		
Reinforcement grade	S420		
Modulus of elasticity of concrete (MPa)	31000		
Modulus of elasticity of steel (MPa)	199947		
Unit weight of rebar (kN/m^3)	76.9		
Unit weight of concrete (kN/m^3)	25		
Soil conditions			
Soil safety stress (kN/m^2)	170		
Soil type (TBEC 2018)	ZC		
Spectrum characteristic periods (s)	T_A=0.061, T_B=0.306		
0.2 s spectral acceleration coefficient (s_s)	1.035		
1.0 s spectral acceleration coefficient (s_1)	0.253		
Short period design spectral acceleration coefficient (s_{ds})	1.242		
Long period design spectral acceleration coefficient (s_{d1})	0.3795		
PGA (g)	0.439		
PGV (cm/s)	25.062		

were assigned to columns to capture the interaction between axial force and biaxial bending moments. Shear hinges were not modeled as the capacity design and detailing ensured flexure-dominated response. The moment-curvature analyses of beams and columns were conducted within SAP2000® to ensure the assigned hinge properties reflected realistic section behavior. Based on these moment-curvature relationships, skeleton curves were automatically generated and assigned to each element, effectively defining the nonlinear hinge properties. In addition to frame elements, the basement walls and floor slabs were modeled using equivalent linear modeling techniques, with section stiffness values adjusted according to the effective stiffness recommendations in TBEC 2018 (2018). Global *P*-delta effects were also included in the analysis to account for second-order geometric nonlinearity. Figures 9a-c show a view of the case study building modeled in SAP2000®.

The column-beam connections were modeled as semi-rigid elements using plastic joints, whereas the shear walls and slabs were rigidly connected to the

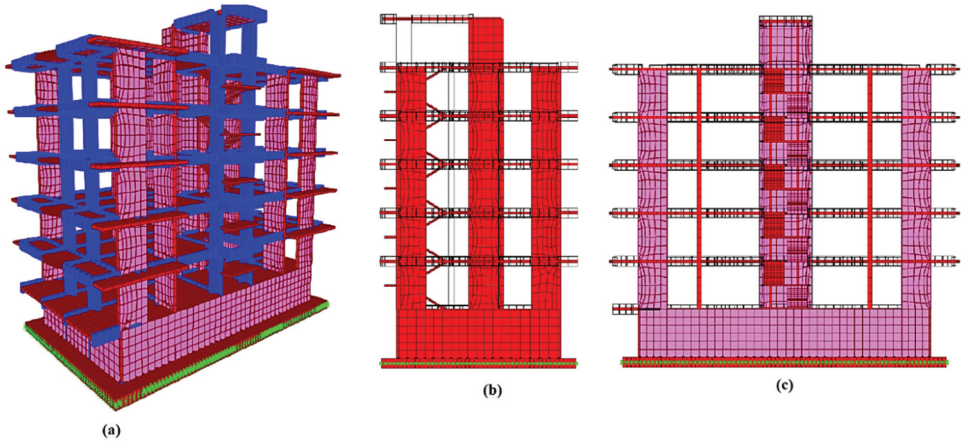

Figure 9. Case study building (a) 3D view, (b) elevation in short direction, and (c) elevation in long direction.

frames through nodal points to ensure a proper force transfer. This approach assumes that the wall and slab elements work together with the frame system and that no separation (e.g. potential pounding) occurs between the elements. The RC shear walls were modeled with shell finite elements, including the degrees of freedom related to both the in-plane and out-of-plane displacements. There were six degrees of freedom at each nodal point of the shell element. As the nodal points of the frame elements also have six degrees of freedom, the shell elements are directly connected to the nodal points of the frame elements.

Soil–structure interactions were considered using a one-parameter Winkler spring model (Bao and Liu 2020; Barzgar Torghabeh, Tehranizadeh, and Taslimi 2023; Farazmand, Behnamfar, and Aziminejad 2025; Tonyali, Ates, and Adanur 2019). In this model, the soil is represented as a series of independent springs, each of which responds only to the loads applied directly above it. The stiffness of these springs is determined by the properties of the soil, such as its bearing capacity and density. This model was selected for its ease of use and efficiency, providing a basic (yet effective) representation of soil–structure interactions. The interaction between the raft foundation and soil was modeled by discretizing the foundation into finite elements, with spring elements assigned to each node. For the ZC soil class, the subgrade reaction value was taken as approximately 30,000 kN/m^3, which was assigned as the spring constant of the Winkler springs.

2.6. Determination of shear strength

Shear failures are common in RC columns during severe earthquakes. Therefore, shear strength is critical for the assessment of structural safety. According to TEC 2007 (2007), the following condition must be satisfied for the shear safety of an RC column:

$$V_r \geq V_d \tag{1}$$

where V_d is the design shear force; and V_r is the shear strength.

The shear strength is obtained by summing the contributions of the concrete (V_c) and shear reinforcement (V_w):

$$V_r = 0.8\left[0.65\, f_{ctd}\, b_w\, d\left(1 + 0.07\frac{N_d}{A_c}\right)\right] + \frac{A_{sw}}{s} f_{ywd}\, d \tag{2}$$

where f_{ctd} is the design tensile strength of the concrete, b_w is the section width perpendicular to the bending direction, d is the section length in the bending direction (effective length), N_d is the design axial force, A_c is the cross-sectional area, A_{sw} is the shear reinforcement area, s is the shear reinforcement spacing, and f_{ywd} is the design yield strength of the shear reinforcement.

3. Structural response under seismic loading

3.1. Pushover analyses

The case study building was subjected to a Nonlinear Static Pushover Analysis as per TBEC 2018 (2018). Previous research has confirmed that such an analysis is adequate to assess the capacity of structures (Chopra and Goel 2002; Krawinkler and Seneviratna 1998; Kurt and Tonyalı 2020). In TBEC 2018, three damage limits are defined: Limited Damage (IO-Immediate Occupancy), Controlled Damage (LS-Life Safety), and Pre-Collapse Damage (CP-Collapse Prevention), as shown in Figure 10. The structural performance was evaluated based on the extent of damage in critical elements. TBEC 2018 (2018) specifies the damage conditions associated with the rotation capacity and damage zones of ductile sections, as listed in Table 4. In Table 4, ϕ_u and ϕ_y are the maximum curvature and yield curvature, respectively; L_p and L_s are the plastic-hinge length and shear span, respectively; and d_b is the diameter of the longitudinal reinforcement. The length of the plastic hinge was defined as half the cross-

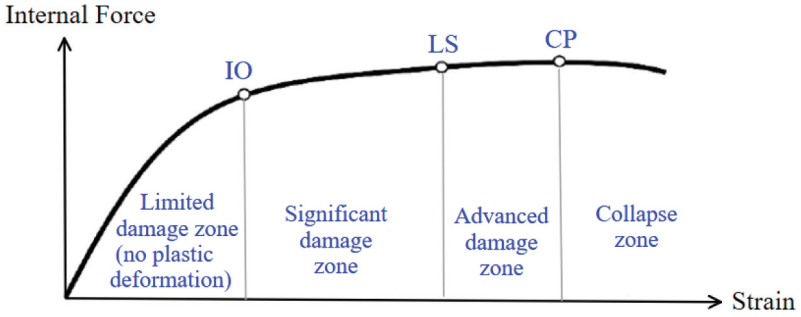

Figure 10. Damage limits in TBEC 2018 (2018).

Table 4. Plastic rotation based on damage limits in TBEC 2018.

Damage limits	Plastic rotations (Q_P)
Immediate Occupancy (IO)	$Q_P^{IO} = 0$
Life Safety (LS)	$Q_P^{LS} = 0.75Q_P^{CD}$
Collapse Prevention (CD)	$Q_P^{CD} = \frac{2}{3}\left[\left(\phi_u - \phi_y\right)L_p\left(1 - 0.5\frac{L_p}{L_s}\right) + 4.5\phi_u d_b\right]$

sectional dimension. Additionally, the vertical loads were calculated using the relationship G + 0.3Q, which multiplies the dead loads (G) by the reduced live loads (Q).

One challenge in pushover analysis is to determine the appropriate target roof displacement (2000; Qi and Moehle 1991). Previous research has suggested that pushover analyses should be carried out until the top roof displacement reaches 2%–3% of the total building height (Kilar and Fajfar 1997; Urbanski et al. 0000). Accordingly, in this study, the target displacement was set as 30 cm for the SAP2000® building model (total height = 20.6 m).

3.2. Nonlinear time-history analyses (NTHAs)

The mainshock ground motion records with the highest peak acceleration values (M_w 7.7, Pazarcik earthquake) from the consecutive 2023 Kahramanmaraş earthquakes (see Appendix A1) were utilized in the NTHAs. Whilst both the M_w 7.7 and M_w 7.6 mainshocks hit the case study building, no visible damage occurred, thus suggesting that the building remained within the elastic range throughout the seismic sequence. In this study, the dynamic analysis was limited to the first mainshock due to the unavailability of reliable ground motion records for the second event. Indeed, the selected acceleration stations did not record usable data for the second mainshock, possibly due to damage or failure of the equipment during the first earthquake. Therefore, the cumulative effects of the seismic sequence could not be explicitly considered in the analysis, and as such this remains a matter of future research.

Table 5 summarizes the main characteristics of the ground motion records used in NTHAs. In this study, the E-W and N-S components of the ground motions were assigned to the structural model's *x* (long) and *y* (short) axes, respectively. This assignment was not based on the actual orientation of the building relative to the fault rupture, as such information was not available. Instead, a consistent directional mapping was assumed for all selected records, wherein the E-W component was mapped to the *x* axis and the N-S component to the *y* axis. For most of the selected ground motion records (see Appendix 1), the N-S component had higher PGA and PGV values compared to the E-W component. To simulate a more critical loading scenario, the stronger ground motion component (N-S) was deliberately assigned to the structurally more flexible (weak) direction (*y* axis). Conversely, the weaker earthquake component (E-W) was applied along the stiffer building direction (*x* axis). The components were combined by adopting 100%

Table 5. Characteristics of ground motion records used in NTHA.

			PGA (g)			PGV (cm/s)		PGA/PGV (g·s/m)	
Station ID	Record details	M_w	E-W	N-S	Up	E-W	N-S	E-W	N-S
S3123	Antakya, 2023 Pazarcık	7.7	0.61	0.66	0.867	104.51	184.82	0.58	0.36
S3124	Antakya, 2023 Pazarcık	7.7	0.65	0.58	0.587	103.78	110.27	0.63	0.53
S3126	Antakya, 2023 Pazarcık	7.7	1.05	1.23	0.922	93.17	110.86	1.13	1.11
S3129	Defne, 2023 Pazarcık	7.7	1.23	1.38	0.716	81.08	164.15	1.52	0.84
S3131	Antakya, 2023 Pazarcık	7.7	0.37	0.37	0.153	43.17	51.83	0.86	0.81
S3141	Antakya, 2023 Pazarcık	7.7	0.88	0.98	0.722	127.64	85.98	0.69	1.14
S4614	Pazarcık, 2023 Pazarcık	7.7	2.22	2.21	1.951	90.89	105.13	2.44	2.10

the earthquake in one direction and ± 30% of the earthquake in the orthogonal direction as per the Turkish code TBEC 2018 (2018).

According to TBEC 2018 and Eq (3), the horizontal earthquake effect E_d can be determined by combining the effects in the x (E_x) and y (E_y) orthogonal directions. For each station in Table 5, the load combinations given in Eq (3) in the x and y directions – a total of eight combinations for both directions – were applied. There were 28 load combinations applied in both the x and y directions of the analysis, for a total of 56 combinations across all stations. In this study, each ground motion record was applied in one principal direction of the building at a time, in accordance with the TBEC 2018 (2018) that prescribes 100% of the component in the principal direction combined with ± 30% of the orthogonal component, as given Eq. (3). Specifically, the E-W component of the record was assigned to the x direction of the building, along with 30% of the N-S component, and vice versa. This approach was adopted to separately investigate the directional performance of the structure under seismic loading. Although both orthogonal components of each ground motion record are available and could technically be applied simultaneously for a more realistic representation of seismic action, the adopted method is consistent with standard engineering practice and allows clearer evaluation of directional structural behavior.

$$E_d{}^{(H)} = \pm E_d{}^{(X)} \pm 0.3E_d{}^{(Y)} \quad (3a)$$

$$E_d{}^{(H)} = \pm 0.3E_d{}^{(X)} \pm E_d{}^{(Y)} \quad (3b)$$

Whilst only the horizontal components (E-W and N-S) of ground motion were considered in the NTHAs, vertical components (i.e. Up direction) recorded at the selected stations exhibited significant amplitudes. For example, the vertical PGA at Station S3123 (closest station to the case study building) was 0.867 g, which exceeds the corresponding horizontal components (0.61g and 0.66g). Similar trends were observed at other stations, such as S4614, where the vertical PGA reached 1.951g. Despite these high values, the vertical input was omitted in the current study as the primary focus was on evaluating the lateral performance of a mid-rise RC building, which does not exhibit vertical irregularities or cantilever elements particularly sensitive to vertical excitation. This modeling approach is consistent with common practice in performance-based seismic evaluation of similar structures (Atmaca et al. 2024; Farsangi and Tasnimi 2016; Khan et al. 2022).

4. Results and discussion

4.1. Pushover analyses results

The results of the pushover analysis in Figure 11a indicate that the building exhibits a higher maximum base shear force in the x direction (20835 kN) than in the y direction (11904 kN). To ensure consistency between the NTHAs and pushover analyses, the same set of ground motion records was used for both procedures. The selected ground motions were first scaled and spectrally matched to the target design spectrum based on their elastic response spectra (Figure 11c). An average elastic spectrum was then computed from the matched records. This average spectrum was subsequently transformed into a demand spectrum in spectral acceleration-displacement format. The pushover analysis results for the performance points were calculated according to ATC-40 (ATC 1996) and are listed in Table 6. The performance point was determined as the intersection between the capacity spectrum (Figure 11b) and the demand spectrum for each principal direction, resulting in Figure 11d. The results indicate that the roof displacement at the performance point was higher in the y direction (0.976 m) than in the x direction (0.482 m). This is reasonable because the y direction of the case study building is more flexible.

Figures 12a-b show the formation of plastic hinges in the building model at the performance points in x (Figure 12a) and y directions (Figure 12b). For clarity, only frame elements are shown in these figures. The results show that all structural elements remained within the Immediate Occupancy (IO) performance level across all displacement steps in both directions. This suggests that the structure sustained minimal damage and retained its operational functionality throughout the analysis period. The fact that no element exceeded the IO state underscores the high seismic resilience of the structure, ensuring safety and usability without requiring major repairs.

4.2. Nonlinear time-history analyses (NTHA) results

4.2.1. Inter-story drift ratios

Figure 13 presents the inter-story drift ratios (IDRs) of the case study building under the selected records, considering both x and y directions (a1–a7 for x direction, b1–b7 for y direction). Each subfigure illustrates the vertical distribution of IDRs over the building's height, with the red dashed line indicating the Immediate Occupancy (IO) performance limit of 1.0% according to FEMA-356 (2000; Pian et al. 2022). In general, most of the IDRs remained below the IO threshold, indicating that the building remained within acceptable deformation limits. The highest IDR in the x direction (~0.8%) was observed at station S3129 under the load combination -Ex + 0.3Ey (Figure 13a4), while the y direction exhibited a peak IDR ~1.5% at the same station for the 0.3Ex + Ey combination (Figure 13b4). Notably, although station S4614 recorded the highest PGA (see Table 5),

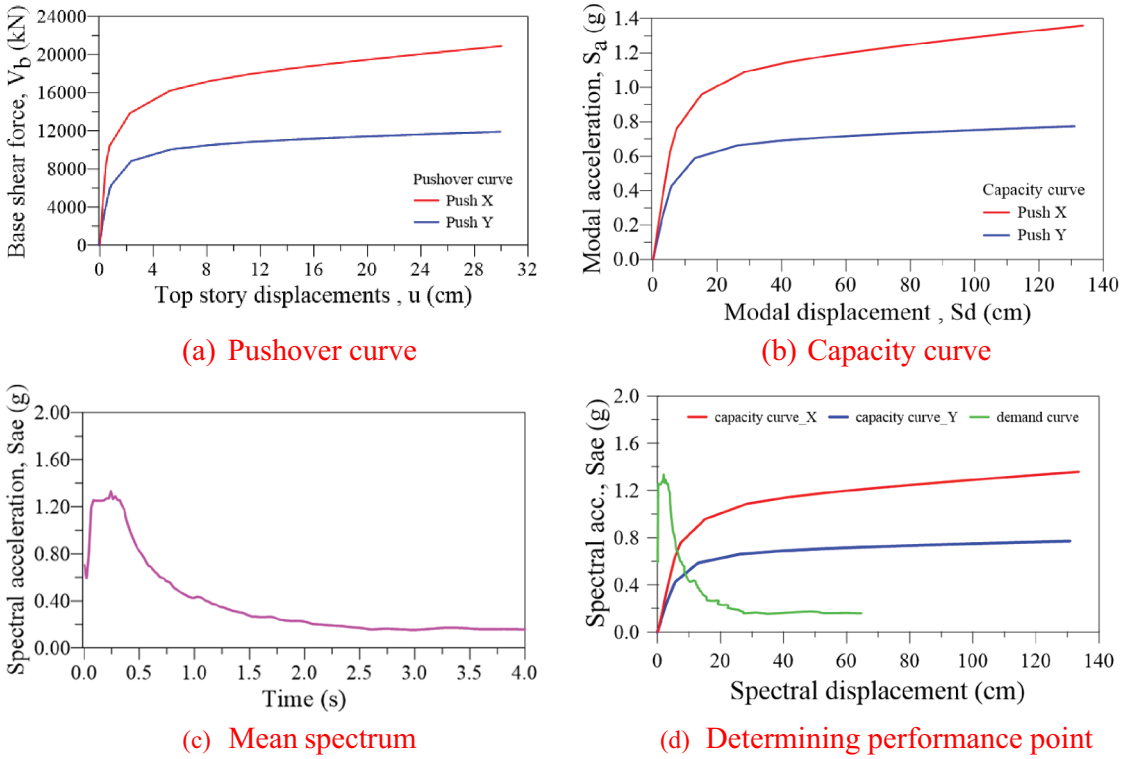

Figure 11. (a) Pushover curves, (b) capacity curves, (c) mean spectrum and (d) performance point of Rende building for *x* and *y* directions.

Table 6. Pushover analysis results.

	Performance point	
	x direction	y direction
Base shear (V)	8674 kN	6490 kN
Roof displacement (D)	0.482 m	0.976 m
Pseudo acceleration (S_a)	0.720g	0.441g
Pseudo displacement (S_d)	6.53 cm	9.55 cm
Effective period (T_{eff})	0.587 s	0.752 s
Damping (β_{eff})	0.064	0.094

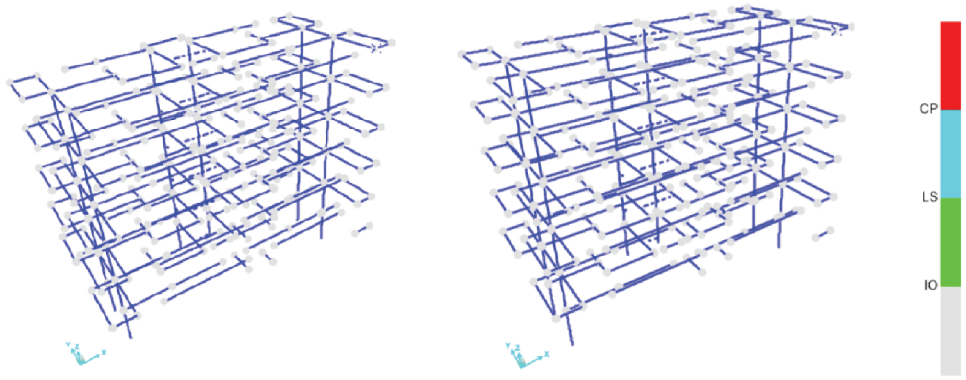

Figure 12. Plastic hinges in the building model, (a) *x* direction, (b) *y* direction.

the maximum IDRs were obtained at station S3129 in both the *x* and *y* directions, even if such station is further away from the building. The largest IDRs recorded at station S3129 can be attributed to the influence of local site effects and/or resonance effects, which increase drifts. Indeed, the dominant frequency of record S3129 in *y* direction (1.5–4.2 Hz) is close to the building's natural frequency (2.12 Hz; see also Figure A3). Overall, the results in Figure 13 show that most of the IDRs remain below the IO performance level. However, since the soil conditions in Hatay province are complex, the IDRs of stations far from the building (e.g., S3129) can exceed the IO drift limit. This suggests that the

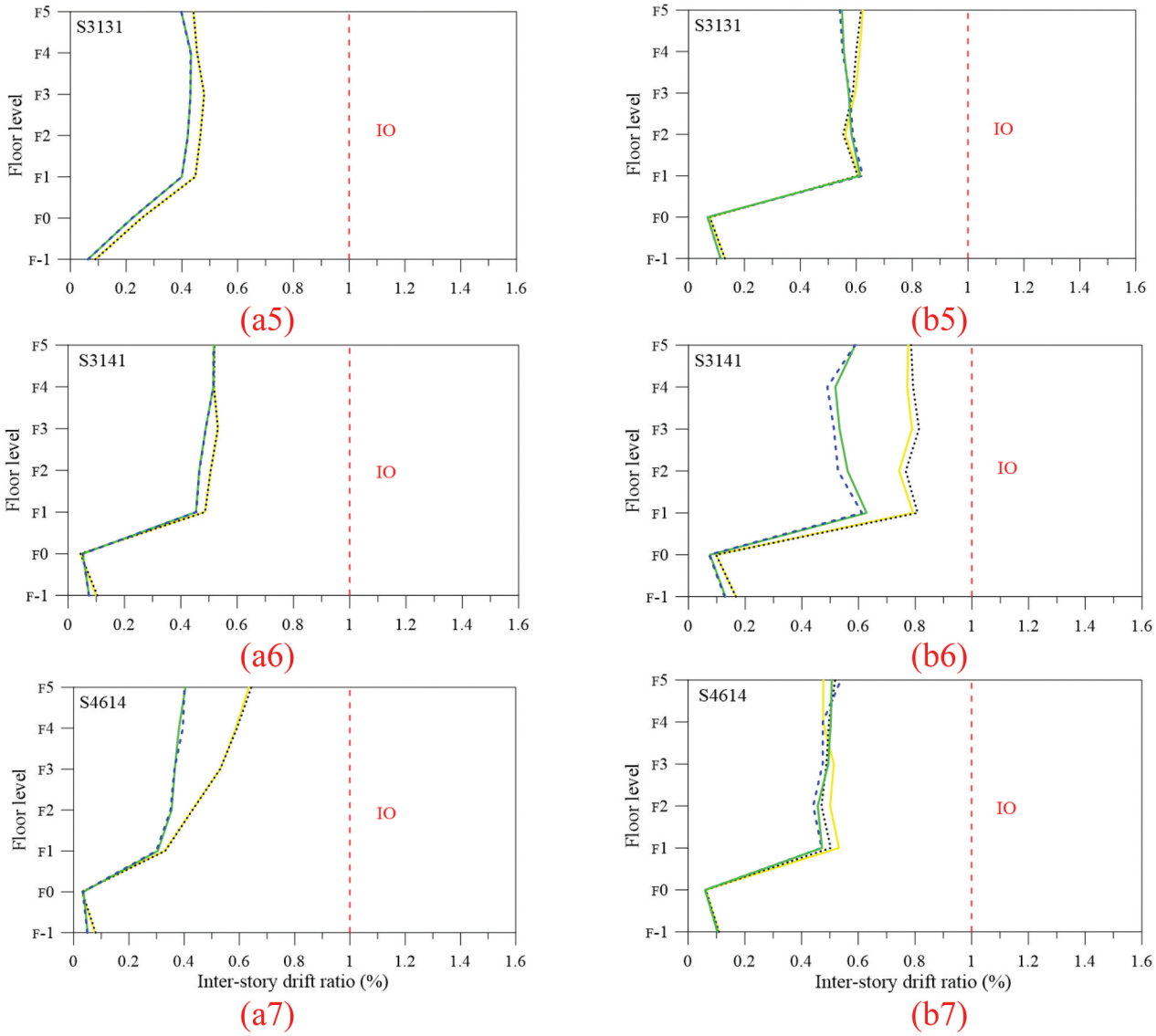

Figure 13. IDRs for selected stations in (a1–a7) *x* direction, and (b1–b7) *y* direction. Each subfigure represents the distribution of IDRs over the building's height. The dashed red line indicates the Immediate Occupancy (IO) performance limit for IDR = 1.0%.

influence of alluvial soils in Hatay province should be carefully considered in the analysis (Kahya et al. 2024; Kiral, Tonyali, and Ergün 2025; Tonyali and Kiral 2024).

4.2.2. Base shear and column/wall shear resistance

Table 7 compares the base shear recorded at the ground floor of the model for different stations, as well as the proportion (%) of shear carried by the RC columns and shear walls. The results in Table 7 indicate that the walls carried approximately 90% of the base shear, whereas the columns resisted approximately 10%. Overall, the maximum base shear force occurred in the *x* direction (17035 kN) under the S3124 record.

Table 8 compares the shear strength (V_r) and shear demand (V_d) of the ground floor columns under record S3124 in the *x* direction and record S3129 in the *y* direction. The results indicate that the shear forces remained below the shear capacities of the columns. The results confirmed the observations made during the post-earthquake survey of the case study building, as no shear damage was observed in the ground floor columns.

4.2.3. Local beam behavior

The condition of beam BG09 is examined here, as it is representative of the rest of the beams in the analyzed building. Figure 14 shows the left and right cross sections at the ends of beam BG09 and their corresponding moment-curvature (*M*-ϕ) relationships. Because the material and dimensional properties of the cross sections are the same and the reinforcement configurations are similar, the *M*-ϕ graphs are also similar. The *M*-ϕ relationships shown in Figure 14 are graphs determined for the bottom reinforcement levels corresponding to the 0° interaction surfaces (IS) of the cross-sections (CS). Table 9 summarizes the values of the *M*-ϕ results, along with

Table 7. Base shear forces at columns and shear walls of ground floor.

		Base shear force													
		S3123		S3124		S3126		S3129		S3131		S3141		S4614	
Elements	Direction	*V*, kN	%	*V*, kN	%	*V*, kN	%	*V*, kN	%	*V*, kN	%	*V*, kN	%	*V*, kN	%
Columns	*x*	1139	9	1454	9	959	9	1426	9	998	9	1038	9	965	9
	y	1538	10	1468	9	956	8	1801	6	1066	9	1367	10	868	9
Shear Walls	*x*	11766	91	15581	91	9577	91	14023	91	9845	91	10553	91	10048	91
	y	14558	90	14173	91	11676	92	26010	94	10303	91	11855	90	9076	91
Total shear force (kN)	*x*	12905		17035		10536		15448		10843		11591		11013	
	y	16095		15640		12632		27810		11368		13222		9943	

Table 8. Shear strength and shear demands of ground floor columns.

Columns	Direction	b_w (mm)	h (mm)	d (mm)	N_d (kN)	V_c (kN)	V_w (kN)	V_r (kN)	V_d (kN)	Control
C1	*x*	900	300	260	782.368	175.634	381.616	557.250	307.803	✓
	y	300	900	860		193.647	473.350	666.997	535.339	✓
C2	*x*	900	300	260	779.566	175.527	381.616	557.143	290.405	✓
	y	300	900	860		193.530	473.350	666.880	592.542	✓
C3	*x*	300	700	660	752.374	154.538	363.269	517.806	299.188	✓
	y	700	300	260		142.050	286.212	428.262	200.798	✓
C4	*x*	300	700	660	755.420	154.663	363.269	517.932	270.014	✓
	y	700	300	260		142.165	286.212	428.377	206.564	✓
C5	*x*	300	700	660	781.670	155.744	363.269	519.013	261.508	✓
	y	700	300	260		143.159	286.212	429.371	184.074	✓
C6	*x*	300	700	660	778.150	155.599	363.269	518.868	231.232	✓
	y	700	300	260		143.026	286.212	429.237	204.037	✓

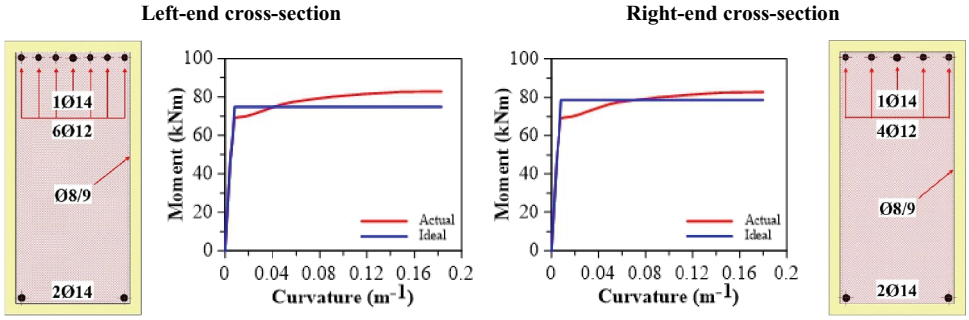

Figure 14. Left and right cross sections at ends of beam BG09 and *M*-ϕ relationships.

the calculated values for the top reinforcement level corresponding to the 180° interaction surface. Table 9 also includes the permissible plastic rotation limit values for different damage performance levels, as specified in TBEC 2018 (2018). The plastic rotation limit values for the collapse prevention ($\theta_p^{(CD)}$), controlled damage ($\theta_p^{(LS)}$), and limited damage ($\theta_p^{(IO)}$) performance levels were calculated based on the equations given in Table 4. Additionally, the table presents the maximum plastic rotation (θ_p) capacities for both end cross sections of the beam. The damage level of the beam can be determined by comparing the plastic rotation limit values with those occurring at the beam ends under the influence of an earthquake. Table 10 lists the plastic rotation values at both ends of the BG09 beam under the influence of each record. The results in Table 10 indicate that the maximum plastic rotations at both ends of the beam occurred under record S3129Y. When comparing the plastic rotation values obtained for all records with the allowable plastic rotation limits, it is evident that all values are below the controlled damage limit. Thus, although the damage severity was slightly higher for S3129Y, only minor damage occurred in the beam for all the records.

4.2.4. Comparison with poorly performing neighbouring buildings

In addition to the case study building itself, it is also worthwhile to consider the seismic response of the neighbouring structures. Low- and mid-rise RC moment frames, as well as hybrid frame-wall systems, suffered extensive damage due to design shortcomings, high drift demands, and a lack of structural walls. Nonetheless, the primary causes of failure in adjacent buildings were attributed to poor concrete quality, substandard materials, inadequate detailing, and deficiencies in the design and construction phases. In contrast, RC wall buildings

Table 9. *M*-ϕ parameters and plastic rotation limits for beam BG09.

											TBEC 2018			
CS	IS	*b* (m)	*h* (m)	d_b (m)	L_s (m)	L_p (m)	ϕ_y (m^{-1})	M_y (kNm)	ϕ_u (m^{-1})	M_u (kNm)	$\theta_p^{(IO)}$ (rad)	$\theta_p^{(LS)}$ (rad)	$\theta_p^{(CD)}$ (rad)	θ_p (rad)
Left end	0°	0.25	0.50	0.0140	1.425	0.25	0.00796	74.777	0.1827	82.734	0.00000	0.02568	0.03424	0.04368
	180°			0.0123			0.00953	202.442	0.2084	208.847	0.00000	0.02845	0.03793	0.04972
Right end	0°	0.25	0.50	0.0140	1.425	0.25	0.00837	78.651	0.1798	82.789	0.00000	0.02521	0.03362	0.04286
	180°			0.0124			0.00892	150.847	0.1878	150.847	0.00000	0.02564	0.03418	0.04472

Table 10. Plastic rotations at the left and right ends of beam BG09 from vs TBEC 2018 limits.

Station	Direction	Left end θ_{pbl} [rad]	Right end θ_{pbr} [rad]	Controlled damage limit (TBEC 2018) $\theta_p^{(LS)}$ [rad]
S3123	*x*	0.00544	0.00290	For left end:
	y	0.00764	0.00361	0.02568
S3124	*x*	0.00803	0.00414	For right end:
	y	0.00720	0.00365	0.02521
S3126	*x*	0.00469	0.00279	
	y	0.00510	0.00318	
S3129	*x*	0.00697	0.00453	
	y	0.01209	0.00536	
S3131	*x*	0.00472	0.00250	
	y	0.00519	0.00334	
S3141	*x*	0.00537	0.00322	
	y	0.00684	0.00367	
S4614	*x*	0.00425	0.00228	
	y	0.00439	0.00296	

performed well if they had an adequate number and orientation of structural walls. Similar behavior was observed in other hybrid frame-wall buildings across Hatay region (Ince 2024; Ivanov and Chow 2023; Mertol et al. 2023; Ozturk, Arslan, and Korkmaz 2023; Sezgin et al. 2024; Sonmez et al. 2025; Turan et al. 2024)

It is worth mentioning that the case study building examined here was built in accordance with new seismic regulations, which suggests that a flexural failure (rather than shear failure) was expected to dominate its behavior. Shear failures often occur if construction flaws or considerable flexural damage exist. Conversely, only one wall of the case study building (located between two doors) had a minor crack after the Kahramanmaraş earthquakes (refer to Figure 7). Additionally, the numerical analysis confirmed that no structural damage occurred in the building, as illustrated in Figure 5.

Whilst numerous studies highlight the superior seismic performance of RC shear wall-frame buildings during earthquakes (Fintel 1991; Kazaz 2025; Sonmez et al. 2025), many of such structures also collapsed during the Kahramanmaraş earthquakes. Collapses in these building can be mainly attributed to: a low wall density index, discontinuities and misalignments in frame axes, insufficient seismic detailing, a unidirectional arrangement of walls, slender wall structures, inadequate boundary confinement, and use of eccentric connections. The following section summarises good practices that led to a high seismic resilience of the case study building.

4.2.5. Lessons learnt and good design practices

The results presented in this study and the post-earthquake field evidence after the Kahramanmaraş earthquakes indicate that RC dual-system buildings can perform better than ductile frames, mainly because the latter have experienced either collapse or substantial damage owing to inherent issues with design and detailing in Türkiye. The good performance of RC dual-system buildings can be largely attributed to the adequate location, large aspect ratio, and robust density of shear walls within the plan of a building. In particular, the shear wall index (ρ) is quantitatively expressed as the ratio of the total cross-sectional area of the walls in one direction $\left(\sum^{A_{wt}}\right)$ to the overall base plan area (A_{pt}):

$$\rho = \frac{A_{wt}}{A_{pt}} = \frac{\sum A_{wi}}{A_{pt}} \tag{4}$$

According to Kazaz (Kazaz 2025), a minimum wall index of 0.6% is necessary to ensure the Life Safety performance level in low-rise RC dual-system buildings. The wall indices for the case study building (see Figure 6) were $\rho = 1.5\%$ $\left(\frac{\text{total shear wall area of ground floor}\left(\sum^{A_{wt}}\right)}{\text{total floor area of ground floor}\left(A_{pt}\right)} = \frac{2.75m^2}{182.9m^2}\right)$ and 1.84% $\left(\frac{3.3625m^2}{182.9m^2}\right)$ in the *x* and *y* directions, respectively. Similarly, Sonmez and Rodriguez (Sönmez and Rodriguez 2024) investigated RC dual-system buildings following the 2023 earthquake in Türkiye. They concluded that RC dual-system buildings with a lateral stiffness index $H/T \geq 32$ in one direction and $H/T \geq 45$ in both directions (H = building height; T = fundamental period) are likely to experience limited damage during severe earthquakes. The case

study Rende building ($H = 20$ m, $T_x = 0.44$ s and $T_y = 0.47$ s) has $H/T = 46.8$ $\left(\frac{20.6m}{0.44s}\right)$ and 43.8 $\left(\frac{20.6m}{0.47s}\right)$ in the x and y directions, respectively, and an average $H/T = 45.3$, which is consistent with the findings of Sönmez et al. (Sönmez and Rodriguez 2024). The relatively high wall index and lateral stiffness index explain why the case study building (as well as the SAP2000® model) remained essentially undamaged when subjected to severe ground motions produced by the Pazarcık records. As a result, it is recommended that the design of a low-rise RC dual-system building adopts the minimum values of the shear wall index ($\rho = 0.6\%$) and average lateral stiffness index ($H/T \geq 45$) suggested by Kazaz (Kazaz 2025) and Sönmez et al. (Sönmez and Rodriguez 2024), respectively. However, future research should verify whether such values are applicable to other RC dual-system buildings with different geometries and materials, such as those studied in this article.

The results of this study, along with the observed performance after past seismic events, confirm that RC dual-system buildings with adequately robust walls can effectively control drift levels and resist severe earthquakes. However, it should be noted that while this study focuses only on a low-rise RC shear wall building, further research should investigate other types of RC shear walls and steel buildings with different soil types and earthquakes. Moreover, additional research should examine the behavior of other types of structures subjected to the Kahramanmaraş earthquakes, such as masonry structures, bridges, or buildings with dampers (Asadpour et al. 2023; Besharatian et al. 2024; Kıral and Gürbüz 2024; Kiral and Tonyali 2024; Kiral, Ergün, et al. 2024; Kiral, Garcia, et al. 2024; Kiral, Gurbuz, and Ustabas 2024; Kiral, Tonyali, and Elias 2025; Wang and Ma 2024).

5. Summary and conclusions

This study investigates the seismic resilience of an existing RC dual-system building designed with TEC 2007 during the Kahramanmaraş earthquakes. A case study building in the Hatay region was modeled using SAP2000® software. The shear wall-frame dual building experienced almost no damage during the earthquakes, whereas all neighboring buildings collapsed. The building was then subjected to static pushover and nonlinear time-history analyses (NTHA) using real ground motions recorded during the Pazarcik earthquake ($M_w = 7.7$), which was the strongest of the two Kahramanmaraş earthquakes. Based on the results of this study, the following conclusions can be drawn:

- Overall, the results from the NTHA indicate that the maximum inter-story drift (IDR) ratios experienced by all floors of the case study building remained below the Immediate Occupancy performance level (IDR = 1.0%). Likewise, the shear demands on all walls and columns and the plastic rotations of beams remained below the limits imposed by the TBEC 2018 design code. The results of pushover analysis confirmed that no plastic hinging occurred in the building model.
- Record S3129 imposed the highest structural demands on the case study building, despite not recording the largest PGA (which was observed at S4614). This can be attributed to its dominant frequency range (1.5–4.2 Hz) which matches the building's fundamental frequency (2.12 Hz). Considering that the case study building remained undamaged, it can be concluded that the selection of earthquake records at Hatay requires careful evaluation due to the existing alluvial deposit.
- The NTHAs confirmed that the case study building remained undamaged following the earthquake, even though the spectral acceleration of record S3123 exceeded the DD2 design spectrum of the more stringent TBEC 2018. This suggests that RC dual-system buildings properly designed and built with the previous Turkish code (TEC 2007) should have resisted the strong shaking produced by the Kahramanmaraş earthquake.
- The limited damage experienced by the RC dual-system building can be largely attributed to its high wall index ($\rho = 1.5\%$ and 1.84% in the x and y directions, respectively) and high average lateral stiffness index ($H/T \geq 45.3$). As a result, it is recommended that the design of a low-rise RC dual-system building adopts the minimum values of the shear wall index ($\rho = 0.6\%$) and average lateral stiffness index ($H/T \geq 45.3$), as suggested by Kazaz (Kazaz 2025) and Sönmez et al. (Sönmez and Rodriguez 2024). However, future research should verify whether such values are applicable to other RC dual-system buildings with different geometries and materials, such as those studied in this article. Moreover, future studies should also investigate if the proposed design indices (i.e. wall index ≥0.6% and $H/T \geq 45$) are applicable to other mid-rise or irregular RC dual-system buildings under various soil conditions

Acknowledgements

The authors would like to express their sincere appreciation to Dr. Mihail Petkovski for his valuable and constructive feedback on the manuscript. Acknowledgement is also extended to Mr. Ahmet Erdem Duran for providing the needed information regarding the case study building.

Finally, the authors are grateful to the anonymous reviewers for their insightful comments and suggestions, which significantly contributed to the improvement of this work.

Author contribution

All authors contributed to the study's origin and plan. Material preparations were performed by [Zeliha TONYALI, Adnan KIRAL, Mustafa ERGUN and Reyes GARCIA]. Data collection was conducted by [Adnan KIRAL and Mustafa ERGUN]. The first draft of the manuscript was partially written and specifically reviewed by all authors and all authors commented on previous versions of the manuscript. All authors read and approved the final manuscript.

Disclosure statement

No potential conflict of interest was reported by the author(s).

Data availability statement

The data generated in this study are available from the corresponding author upon reasonable request.

References

AFAD. 2023a. "Disaster and Emergency Management Presidency of Turkey."[Online]. https://www.afad.gov.tr/.

AFAD. 2023b. "Disaster and Emergency Management Presidency of Turkey." Kahramanmaraş'ta Meydana Gelen Depremler HK – Basın Bülteni 36. [Online]. https://www.afad.gov.tr/kahramanmarasta-meydana-gelen-depremler-hk-36 .

Akinci, A., A. A. Dindar, I. E. Bal, D. Ertuncay, E. Smyrou, and D. Cheloni. 2025. "Characteristics of Strong Ground Motions and Structural Damage Patterns from the February 6th, 2023 Kahramanmaraş Earthquakes, Türkiye." *Natural Hazards* 121 (2): 1209–1239. https://doi.org/10.1007/s11069-024-06856-y.

Altunişik, A. C., M. E. Arslan, V. Kahya, B. Aslan, T. Sezdirmez, G. Dok, O. Kirtel. 2023. "Field Observations and Damage Evaluation in Reinforced Concrete Buildings After the February 6th, 2023, Kahramanmaraş–Türkiye Earthquakes." *Journal of Earthquake and Tsunami* 17 (6): 2350024. https://doi.org/10.1142/S1793431123500240.

Asadpour, G., P. Asadi, R. Garcia, and I. Hajirasouliha. 2023. "A Novel Stochastic Linearization Technique for Structures with Nonlinear Fluid Viscous Dampers Including Soil-Structure Interaction." *Journal of Building Engineering* 72:106668. https://doi.org/10.1016/j.jobe.2023.106668.

ASCE 41-17. 2017. Seismic Evaluation and Retrofit of Existing Buildings. Reston, VA, (ASCE).

Asgari, A., and M. H. Bagheripour. 2010. "Earthquake Response Analysis of Soil Layers Using HFTD Approach." *Soil Dynamics and Earthquake Engineering*: 320–325. https://doi.org/10.1061/41102(375)39.

Asgari, A., F. Ranjbar, and M. Bagheri. 2025. "Seismic Resilience of Pile Groups to Lateral Spreading in Liquefiable Soils: 3D Parallel Finite Element Modeling." *Structures* 74:108578. 04/1/2025. https://doi.org/10.1016/j.istruc.2025.108578.

Askan, A., A. Altindal, M. F. Aydin, M. A. Erberik, M. K. Koçkar, M. Tun, M. Senol Balaban, H. Uygucgil, A. Kop, and S. Karimzadeh. 2025. "Assessment of Urban Seismic Resilience of a Town in Eastern Turkiye: Turkoglu, Kahramanmaras Before and After 6 February 2023 M 7.8 Kahramanmaras Earthquake." *Earthquake Spectra* 41 (1): 146–175. https://doi.org/10.1177/87552930241274715.

ATC. 1996. "Seismic Evaluation and Retrofit of Concrete Buildings—Volume 1 (ATC-40). Report No. SSC 96-01."

Atmaca, B., A. C. Altunişik, E. Ertürk Atmaca, H. B. Başağa, M. Günaydin, S. Adanur, Ş. Ateş. 2025. "What Is the Reason for Collapses on February 6, 2023 Kahramanmaraş Earthquakes: Insights from a Dataset of 400 Collapsed RC Buildings Post-Earthquake Analysis." *Journal of Building Engineering* 107:112660. 08/1/2025. https://doi.org/10.1016/j.jobe.2025.112660.

Atmaca, B., E. Ertürk Atmaca, B. Roudane, O. Güleş, E. Demlrkaya, B. Aykanat, A. C. Altunişik, M. Günaydin, M. E. Arslan, and V. Kahya. 2024. "Field Observations and Numerical Investigations on Seismic Damage Assessment of RC and Masonry Minarets During the February 6th, 2023, Kahramanmaraş (Mw 7.7 Pazarcık and Mw 7.6 Elbistan) Earthquakes in Türkiye." *International Journal of Architectural Heritage*: 1–26. https://doi.org/10.1080/15583058.2024.2337651.

Bao, T., and Z. L. Liu. 2020. "Evaluation of Winkler Model and Pasternak Model for Dynamic Soil-Structure Interaction Analysis of Structures Partially Embedded in Soils." *International Journal of Geomechanics* 20 (2): 04019167. https://doi.org/10.1061/(ASCE)GM.1943-5622.0001519.

Barzgar Torghabeh, A., M. Tehranizadeh, and A. Taslimi. 2023. "Probability of Collapse Evaluation for High-Rise Reinforced Concrete Buildings in the Event of Near-Fault Earthquakes and Soil-Structure Interaction Effects." *Structures* 55:1675–1691. https://doi.org/10.1016/j.istruc.2023.06.113.

Bas, S., J. Hunt, B. Gencturk, E. Jampole, Y. B. Sonmezer, B. Chancellor, P. Bassal, M. Celiker, N. Apaydin, and H. Sezen. 2024. "Seismic Performance and Damage Assessment of Bridges During the 2023 Kahramanmaras, Türkiye Earthquakes (M W= 7.8, M W= 7.6)." *Earthquake Spectra* 40 (4): 2339–2363. https://doi.org/10.1177/87552930241262043.

Besharatian, B., H. Tajmir Riahi, R. Garcia, and I. Hajirasouliha. 2024. "A Practical Optimisation Method for Friction Tuned Mass Dampers in Multi-Storey Buildings Subjected to Earthquake Excitations." *Soil Dynamics and Earthquake Engineering* 184:108857. https://doi.org/10.1016/j.soildyn.2024.108857.

Buckreis, T. E., R. Pretell, A. Sandikkaya, Ö. Kale, A. Askan, S. J. Brandenberg, and J. P. Stewart. 2024. "February 6, 2023 Türkiye Earthquakes: Ground Motions." *Japanese Geotechnical Society Special Publication* 10 (11): 282–287. https://doi.org/10.3208/jgssp.v10.SS-6-04.

Büyüktopcu, E. "Bizi Öldüren Deprem Değil: Yeni Değil Yeniden Antakya." https://areteportal.com/bizi-olduren-deprem-degil-yeni-degil-yeniden-antakya/.

Car, E., S. Oller, and E. Oñate. 2000. "An Anisotropic Elastoplastic Constitutive Model for Large Strain Analysis of Fiber Reinforced Composite Materials." *Computer Methods in Applied Mechanics and Engineering* 185 (2–4): 245–277. https://doi.org/10.1016/S0045-7825(99)00262-5.

Chopra, A. K., and R. K. Goel. 2002. "A Modal Pushover Analysis Procedure for Estimating Seismic Demands for Buildings." *Earthquake Engineering and Structural Dynamics* 31 (3): 561–582. https://doi.org/10.1002/eqe.144.

Demir, S., M. Günaydin, B. Atmaca, A. C. Altunişik, M. Hüsem, S. Adanur, Z. Angin, and Ş. Ateş. 2021. "Performance Evaluation of Reinforced Concrete Buildings During the Sivrice-Elazığ Earthquake (Mw=6.8, January 24, 2020) in Accordance with Turkish Earthquake Code." *Journal of Earthquake and Tsunami* 15 (4): 2150018. https://doi.org/10.1142/s1793431121500184.

Er, A. 2025. "Structural Assessment of Earthquake Resilience in Historic Mosques: A Study on Şimşirli Mosque." *Journal of Asian Architecture & Building Engineering*: 1–19. https://doi.org/10.1080/13467581.2025.2465813.

Erdik, M., M. B. D. Tümsa, A. Pınar, E. Altunel, and A. C. Zülfikar. 2023. A preliminary report on the earthquakes in Türkiye. http://doi.org/10.32858/temblor.297 .

Erkek, H., and M. Yetkin. 2023. "Assessment of the Performance of a Historic Minaret During the Kahramanmaraş Earthquakes (Mw 7.7 and Mw 7.6)." *Structures* 58:105620. https://doi.org/10.1016/j.istruc.2023.105620.

Eurocode 8: Design of Structures for Earthquake Resistance – Part 1: General Rules, Seismic Actions and Rules for Buildings. 2004. *EN 1998-1:2004*, E. C. F. Standardization.

Fan, Y., Z. Zhu, and F. Zhang. 2025. "Effect of Different Tailings' Relative Density Modes on Dynamic Response of Tailing Reservoir: A Case Study." *Mining, Metallurgy & Exploration*, 1–20. https://doi.org/10.1007/s42461-025-01224-1.

Farazmand, M., F. Behnamfar, and A. Aziminejad. 2025. "Seismic Response of Structures on Flexible Base Under Foundation Uplift Augmented by Vertical Component of Near-Field Ground Motions." *Soil Dynamics and Earthquake Engineering* 191:109278. https://doi.org/10.1016/j.soildyn.2025.109278.

Farsangi, E. N., and A. A. Tasnimi. 2016. "The Influence of Coupled Horizontal–Vertical Ground Excitations on the Collapse Margins of Modern RC-MRFs." *International Journal of Advanced Structural Engineering (IJASE)* 8 (2): 169–192. https://doi.org/10.1007/s40091-016-0122-0.

FEMA-356. 2000. "Prestandard and Commentary for the Seismic Rehabilitation of Buildings." *Federal Emergency Management Agency*, Washington, DC, USA.

Fintel, M. 1991. "Shearwalls-An Answer for Seismic Resistance?" *Concrete International* 13 (7).

Garcia, R., I. Hajirasouliha, and K. Pilakoutas. 2010. "Seismic Behaviour of Deficient RC Frames Strengthened with CFRP Composites." *Engineering Structures* 32 (10): 3075–3085. 10/1/2010. https://doi.org/10.1016/j.engstruct.2010.05.026.

Ibrahim, A. R., D. A. Makhloof, and X. Ren. 2024. "Seismic Performance and Collapse Analysis of RC Framed-Wall Structure Excited with Turkey/Syria Destructive Earthquake." *Structures* 59:105774. 01/1/2024. https://doi.org/10.1016/j.istruc.2023.105774.

I. Computers and Structures. 2024. "CSI Analysis Reference Manual."

Ince, O. 2024. "Structural Damage Assessment of Reinforced Concrete Buildings in Adıyaman After Kahramanmaraş (Türkiye) Earthquakes on 6 February 2023." *Engineering Failure Analysis* 156:107799. https://doi.org/10.1016/j.engfailanal.2023.107799.

Inel, M., B. T. Cayci, and E. Meral. 2018. "Nonlinear Static and Dynamic Analyses of RC Buildings." *International Journal of Civil Engineering* 16 (9): 1241–1259. 09/1 2018. https://doi.org/10.1007/s40999-018-0285-0.

Işık, E., F. Avcil, E. Arkan, A. Büyüksaraç, R. İzol, and M. Topalan. 2023. "Structural Damage Evaluation of Mosques and Minarets in Adıyaman Due to the 06 February 2023 Kahramanmaraş Earthquakes." *Engineering Failure Analysis* 151:107345. https://doi.org/10.1016/j.engfailanal.2023.107345.

Ivanov, M. L., and W.-K. Chow. 2023. "Structural Damage Observed in Reinforced Concrete Buildings in Adiyaman During the 2023 Türkiye Kahramanmaraş Earthquakes." *Structures* 58:105578. 12/1/2023. https://doi.org/10.1016/j.istruc.2023.105578.

Jin, L., M. Fan, W. Yu, C. Xie, and X. Du. 2025. "Effect of Fibre Content on Low-Temperature Failure Strength and Toughness of Different Sized BFRC Under Static and Dynamic Loadings: An Experimental Study." *Engineering Fracture Mechanics* 314:110737. https://doi.org/10.1016/j.engfracmech.2024.110737.

Kahya, V., A. F. Genç, F. Sunca, B. Roudane, A. C. Altunişik, S. Yilmaz, M. Günaydin, G. Dok, O. Kirtel, and A. Demir. 2024. "Evaluation of Earthquake-Related Damages on Masonry Structures Due to the 6 February 2023 Kahramanmaraş-Türkiye Earthquakes: A Case Study for Hatay Governorship Building." *Engineering Failure Analysis* 156:107855. https://doi.org/10.1016/j.engfailanal.2023.107855.

Kap, T. 2025. "The Effects of Reinforced Concrete Shear Wall on the Earthquake Behaviour of the Buildings with Various Column Sections." *Journal of Asian Architecture & Building Engineering*: 1–15. https://doi.org/10.1080/13467581.2025.2467252.

Kazaz, İ. 2025. "Evaluation of Seismic Performance, Design and Practice of Frame-Wall Buildings in Türkiye After the 6 February 2023 Kahramanmaraş Earthquakes." *Journal of Building Engineering* 99:111557. 04/1/2025. https://doi.org/10.1016/j.jobe.2024.111557.

Kazaz, İ., Ö. Avşar, and A. Dilsiz. 2024. "Importance of Building Inspection on the Seismic Response of a Severely Damaged RC Structure During the February 6, 2023 Kahramanmaraş Earthquake Sequence." *Engineering Failure Analysis* 162:108410. https://doi.org/10.1016/j.engfailanal.2024.108410.

Khan, F. A., M. Rashid, S. W. Khan, M. Rizwan, Y. I. Badrashi, M. Fahim, M. A. Tanoli, W. Khaliq, and A. Gul. 2022. 'Comparative Seismic Performance Assessment of RC and RC/ECC Hybrid Frame Structures: A Shake Table Study." *Innovative Infrastructure Solutions* 7 (1): 1–17. https://doi.org/10.1007/s41062-021-00692-w.

Kilar, V., and P. Fajfar. 1997. "Simple Push-Over Analysis of Asymmetric Buildings." *Earthquake Engineering and Structural Dynamics* 26 (2): 233–249. https://doi.org/10.1002/(SICI)1096-9845(199702)26:2<233::AID-EQE641>3.0.CO;2-A.

Kiral, A., M. Ergün, Z. Tonyali, M. Artar, and İ. Şentürk. 2024. "A Case Study Comparing Seismic Retrofitting Techniques for a Historically Significant Masonry Building's Minaret." *Engineering Failure Analysis* 166:108873. 12/1/2024. https://doi.org/10.1016/j.engfailanal.2024.108873.

Kiral, A., R. Garcia, M. Petkovski, and I. Hajirasouliha. 2024. "Seismic Performance Assessment of Steel Buildings Equipped with a New Semi-Active Displacement-Dependent Viscous Damper." *Journal of Earthquake and Tsunami* 18 (6): 2450022. https://doi.org/10.1142/s1793431124500222.

Kıral, A., and A. Gürbüz. 2024. "Using Supplemental Linear Viscous Dampers for Experimentally Verified Base-Isolated Building: Case Study." *Journal of Structural Engineering & Applied Mechanics (Online)* 7 (1): 34–50. https://doi.org/10.31462/jseam.2024.01034050.

Kiral, A., A. Gurbuz, and I. Ustabas. 2024. "The Seismic Response Evaluation of an Existing Multi-Span Reinforced Concrete Highway Bridge in the Presence of Linear and

Nonlinear Viscous Dampers." *Arabian Journal for Science & Engineering*. July, 2. https://doi.org/10.1007/s13369-024-09265-2.

Kiral, A., and Z. Tonyali. 2024. "The Effect of LRB Stiffness Changes with and without Supplemental Viscous Dampers on Seismic Responses of an Experimentally Verified MDOF Building." *Sigma Journal of Engineering and Natural Sciences* 43 (1): 301–315. https://doi.org/10.14744/sigma.2024.00104.

Kiral, A., Z. Tonyali, and S. Elias. 2025. "Optimizing Seismic Performance of Base-Isolated Buildings with Mass and Stiffness Variations Under Near and Far Fault Ground Motions." *Structures* 76: Elsevier, p. 109026. https://doi.org/10.1016/j.istruc.2025.109026.

Kiral, A., Z. Tonyali, and M. Ergün. 2025. "A Comprehensive Analysis of the Ground Motions of the 2023 Kahramanmaraş, Türkiye Earthquakes." *Earthquake and Structures* (26). https://doi.org/10.12989/eas.2025.28.3.203.

Krawinkler, H., and G. Seneviratna. 1998. "Pros and Cons of a Pushover Analysis of Seismic Performance Evaluation." *Engineering Structures* 20 (4–6): 452–464. https://doi.org/10.1016/S0141-0296(97)00092-8.

Kurt, Z., and Z. Tonyalı. 2020. "Performance Analysis of a Reinforced Concrete Frame System According to TBEC-2018." *Sciennovation* 1 (2): 6–22.

Lagos, R., M. Kupfer, J. Lindenberg, P. Bonelli, R. Saragoni, T. Guendelman, L. Massone, R. Boroschek, and F. Yanez. 2012. "Seismic Performance of High-Rise Concrete Buildings in Chile." *International Journal of High-Rise Buildings* 1 (3): 181–194. https://doi.org/10.21022/IJHRB.2012.1.3.181.

Lashgari, A., M. R. Soghrat, Y. Jafarian, and H. Zafarani. 2024. "The 2023 Turkey–Syria Earthquake Sequence: Ground-Motion and Local Site-Effect Analyses for Kahramanmaras City." *International Journal of Civil Engineering* 22 (5): 877–899. https://doi.org/10.1007/s40999-023-00917-2.

Mander, J. B., M. J. N. Priestley, and R. Park. 1988. "Theoretical Stress-Strain Model for Confined Concrete." *Journal of Structural Engineering* 114 (8): 1804–1826. https://doi.org/10.1061/(ASCE)0733-9445(1988)114:8(1804).

Mardani, A., H. G. Şahin, and Y. Kaya. 2024. "Effect of the Kahramanmaraş Earthquake on Standing Water Tanks in the Adana Region and Buildings in Hatay-Antakya." *Engineering Science and Technology, an International Journal* 55:101744. https://doi.org/10.1016/j.jestch.2024.101744.

Mertol, H. C., G. Tunç, T. Akış, Y. Kantekin, and İ. C. Aydın. 2023. "Investigation of RC Buildings After 6 February 2023, Kahramanmaraş, Türkiye Earthquakes." *Buildings* 13 (7): 1789. https://doi.org/10.3390/buildings13071789.

Onat, O., F. Deniz, A. Özmen, E. Özdemir, and E. Sayın. 2023. "Performance Evaluation and Damage Assessment of Historical Yusuf Ziya Pasha Mosque After February 6, 2023 Kahramanmaras Earthquakes." *Structures* 58:105415. 12/1/2023, doi: https://doi.org/10.1016/j.istruc.2023.105415.

Onder Cetin, K., F. Cuceoglu, B. U. Ayhan, S. Yildirim, S. Aydin, S. Demirdogen, Y. Er, A. Gurbuz, and R. E. S. Moss. 2024. "Performance of Hydraulic Structures During 6 February 2023 Kahramanmaraş, Türkiye, Earthquake Sequence." *Earthquake Spectra* 40 (4): 2231–2267. https://doi.org/10.1177/87552930241258295.

Över, S., A. Büyüksaraç, Ö. Bekta, and A. Filazi. 2011. "Assessment of Potential Seismic Hazard and Site Effect in Antakya (Hatay Province), SE Turkey." *Environmental Earth Sciences* 62:313–326. https://doi.org/10.1007/s12665-010-0525-3.

Ozdemir, A. 2024. "Examining the Effect of Structural Characteristics of Antakya Building Stock on the Damage Level After the Kahramanmaraş Earthquakes." *Journal of Earthquake Engineering*: 1–30. https://doi.org/10.1080/13632469.2024.2390088.

Ozkul, T. A., A. Kurtbeyoglu, M. Borekci, B. Zengin, and A. Kocak. 2019. "Effect of Shear Wall on Seismic Performance of RC Frame Buildings." *Engineering Failure Analysis* 100:60–75. 06/1/2019. https://doi.org/10.1016/j.engfailanal.2019.02.032.

Ozturk, M., M. H. Arslan, G. Dogan, A. S. Ecemis, and H. D. Arslan. 2023. "School Buildings Performance in 7.7 MW and 7.6 MW Catastrophic Earthquakes in Southeast of Turkey." *Journal of Building Engineering* 79:107810. https://doi.org/10.1016/j.jobe.2023.107810.

Ozturk, M., M. H. Arslan, and H. H. Korkmaz. 2023. "Effect on RC Buildings of 6 February 2023 Turkey Earthquake Doublets and New Doctrines for Seismic Design." *Engineering Failure Analysis* 153:107521. https://doi.org/10.1016/j.engfailanal.2023.107521.

Pan, R., C. Xu, K. Jia, P. Dou, and I. Kamran. 2023. "Large-Scale Shaking Table Test and Three-Dimensional Numerical Simulation Research on Earthquake Seismic Failure Response of Laterally Spreading Site-Pile Group-Superstructure System." *Bulletin of Earthquake Engineering* 21 (10): 4789–4819. https://doi.org/10.1007/s10518-023-01713-y.

Pian, C., E. V. Muho, J. Qian, and D. E. Beskos. 2022. "A Hybrid Force/Displacement Seismic Design Method for Reinforced Concrete Infilled-MRFs and Wall-Frame Dual Systems." *Journal of Earthquake Engineering* 26 (6): 2731–2753. https://doi.org/10.1080/13632469.2020.1785358.

Prince, M. B., M. N. I. Mollah, M. R. A. Chowdhury, and D. Sen. 2023. "Comparison of Lateral Behavior of an Existing RC Building Under Nonlinear Static and Incremental Dynamic Loads." *Asian Journal of Civil Engineering* 24 (7): 2155–2164. 11/1 2023. https://doi.org/10.1007/s42107-023-00632-2.

Pujol, S., I. Bedirhanoglu, C. Donmez, J. D. Dowgala, M. Eryilmaz-Yildirim, K. Klaboe, F. B. Koroglu, R. D. Lequesne, B. Ozturk, and L. Pledger. 2024. "Quantitative Evaluation of the Damage to RC Buildings Caused by the 2023 Southeast Turkey Earthquake Sequence." *Earthquake Spectra* 40 (1): 505–530. https://doi.org/10.1177/87552930231211208.

Qi, X., and J. P. Moehle. 1991. *Displacement Design Approach for Reinforced Concrete Structures Subjected to Earthquakes*. Earthquake Engineering Research Center, College of Engineering, University of California, Berkeley, USA.

Sagbas, G., R. Sheikhi Garjan, K. Sarikaya, and D. Deniz. 2024. "Field Reconnaissance on Seismic Performance and Functionality of Turkish Industrial Facilities Affected by the 2023 Kahramanmaras Earthquake Sequence." *Bulletin of Earthquake Engineering* 22 (1): 227–254. https://doi.org/10.1007/s10518-023-01741-8.

SBP. 2023. "Türkiye Recovery and Reconstruction Assessment (TERRA). Türkiye Earthquakes Recovery and Reconstruction Assessment. Report with the Support of the United Nations and the European Union, with Select Inputs from World Bank Staff." Strategy and Budget Presidency (SBP). [Online]. https://www.sbb.gov.tr/wp-content/uploads/2023/03/Turkiye-Recovery-and-Reconstruction-Assessment.pdf.

Sezgin, S. K., G. B. Sakcalı, S. Özen, E. Yıldırım, E. Avcı, B. Bayhan, and N. Çağlar. 2024. "Reconnaissance Report on Damage Caused by the February 6, 2023,

Kahramanmaraş Earthquakes in Reinforced-Concrete Structures." *Journal of Building Engineering* 89:109200. https://doi.org/10.1016/j.jobe.2024.109200.

Sonmez, E., M. Eryilmaz Yildirim, M. F. Aydin, and F. B. Koroglu. 2025. "Seismic Performance Assessment of Structural Systems in the Aftermath of the 2023 Kahramanmaraş Earthquakes: Observations and Fragility Analyses." *Earthquake Spectra* 41 (1): 198–218. https://doi.org/10.1177/87552930241287541.

Sönmez, E., and M. E. Rodriguez. 2024. "Frame Buildings Are Not an Answer for Earthquakes: The Case of the February 2023 Earthquakes in Türkiye." *Earthquake Spectra* 40 (4): 2364–2382. https://doi.org/10.1177/87552930241262753.

Stockwell, R. G., L. Mansinha, and R. P. Lowe. 1996. "Localization of the Complex Spectrum: The S Transform." *IEEE Transactions on Signal Processing* 44 (4): 998–1001. https://doi.org/10.1109/78.492555.

TEC. 2007. Turkish Earthquake Resistant Design Code Ministry of Public Works and Settlement. *Ankara*.

Tonyali, Z., E. L. Alemdağ, and G. T. Kibar. 2024. "Evaluation of Seismic Response of the Cross-Laminated Timber (CLT) Multi-Storey Residential Building Under the February 6, 2023, Kahramanmaraş Earthquakes." *Journal of Architectural Sciences and Applications* 9 (Special Issue): 41–63. https://doi.org/10.30785/mbud.1338909.

Tonyali, Z., S. Ates, and S. Adanur. 2019. "Spatially Variable Effects on Seismic Response of the Cable-Stayed Bridges Considering Local Soil Site Conditions." *Structural Engineering and Mechanics* 70 (2): 143–152. https://doi.org/10.12989/sem.2019.70.2.143.

Tonyali, Z., and A. Kiral. 2024. "Evaluation of Earthquake-Related Damages on the Reinforced Concrete Buildings Due to the February 6, 2023, Kahramanmaras-Turkiye Earthquakes." *Recep Tayyip Erdoğan University Journal of Science and Engineering* 5 (1): 89–114. https://doi.org/10.53501/rteufemud.1471964.

Toprak, S., B. P. Wham, E. Nacaroglu, M. Ceylan, and O. Dal. 2025. "Performance of Water Systems During the February 6th Kahramanmaras Earthquakes." *Earthquake Spectra* 41 (1): 322–353. https://doi.org/10.1177/87552930241293571.

Turan, A. I., A. Celik, A. Kumbasaroglu, and H. Yalciner. 2024. "Assessment of Reinforced Concrete Building Damages Following the Kahramanmaraş Earthquakes in Malatya, Turkey (February 6, 2023)." *Engineering Science and Technology, an International Journal* 54:101718. https://doi.org/10.1016/j.jestch.2024.101718.

Turkish Earthquake Building Code, Specifications for buildings to be built in seismic areas. 2018. *Ministry of Public Works and Settlement*. Turkish Disaster and Emergency Management Authority,(AFAD), Ankara, Turkey.

Urbanski, A., E. Spacone, M. Belgasmia, J. L. Sarf, and T. Zimmermann. "Static Pushover Analysis Report 070202."

Vielma, J. C., A. H. Barbat, and S. Oller. 2010. "Seismic Safety of Low Ductility Structures Used in Spain." *Bulletin of Earthquake Engineering* 8 (1): 135–155. https://doi.org/10.1007/s10518-009-9127-4.

Vuran, E., C. Serhatoğlu, M. Ö. Timurağaoğlu, E. Smyrou, İ. E. Bal, and R. Livaoğlu. 2025. "Damage Observations of RC Buildings from 2023 Kahramanmaraş Earthquake Sequence and Discussion on the Seismic Code Regulations." *Bulletin of Earthquake Engineering* 23 (3): 1153–1182. https://doi.org/10.1007/s10518-023-01843-3.

Wang, Y., and H. Ma. 2024. "Multi-Objective Stochastic Optimization of Tuned Mass Dampers Under Earthquake Excitation Considering Soil–Structure Interaction." *Journal of Asian Architecture and Building Engineering* 23 (5): 1596–1611. https://doi.org/10.1080/13467581.2023.2270754.

Worden, C. B., M. T. Eric, G. H. Michael, and D. J. W. 2020. "Shakemap 4.0 Manual." *United States Geological Survey*. [Online]. http://usgs.github.io/shakemap/.

Xu, W., Y. Zhao, W. Yang, J. Zhang, and D. Chen. 2023. "Seismic Performance of RC Frame-Shear Wall Dual Structural Systems." *Structures* 58:105610. https://doi.org/10.1016/j.istruc.2023.105610.

Yılmaz, Ç. M. 2025. "A Novel Approach to Motor Imagery EEG Signal Transformation and Classification Using Stockwell Transform and Deep Learning Models." *Karadeniz Fen Bilimleri Dergisi* 15 (1): 152–170. https://doi.org/10.31466/kfbd.1509850.

Yön, B., İ. Ö. Dedeoğlu, M. Yetkin, H. Erkek, and Y. Calayır. 2024. "Evaluation of the Seismic Response of Reinforced Concrete Buildings in the Light of Lessons Learned from the February 6, 2023, Kahramanmaraş, Türkiye Earthquake Sequences." *Natural Hazards*, 1–37. https://doi.org/10.1007/s11069-024-06859-9.

Appendix A

A1. *Analysis of recorded ground motions*

In this study, raw (i.e., not filtered) ground motion data during the 06 February Kahramanmaraş earthquakes were taken from the AFAD (AFAD 2023a) database. Table A1 shows the five largest earthquakes in the region and some of the largest accelerations recorded at nearby stations as of 31 March 2023, respectively. The largest PGA was recorded at the Pazarcik station (S4614) of Kahramanmaraş Province and was approximately 2.0 g in all directions. The ground velocity records obtained from the AFAD database indicated that some of the PGVs at the stations in both horizontal directions were up to 170 cm/s. According to the Shakemap Intensity (Worden et al. 2020), ground accelerations exceeding 1.4 g or ground velocities above 180 cm/s are typically associated with a high probability of severe structural damage and significant disruptions to lifelines. These data highlight the extreme intensity of earthquakes and their potential for widespread destruction.

Table A1. Earthquakes at Kahramanmaraş province and its vicinity on 6 February 2023 (AFAD 2023a).

Record ID	Event (d/m/y, time)	Province	District	Lat. [°]	Long. [°]	Magnitude [M_w]	Depth [km]
543428	6 February 2023, 04:17	Kahramanmaraş	Pazarcik	37.288	37.043	7.7	8.6
543431	6 February 2023, 04:28	Gaziantep	Nurdağı	37.304	36.920	6.6	6.2
543430	6 February 2023, 04:36	Gaziantep	Islahiye	37.128	36.639	5.7	11.19
543593	6 February 2023, 13:24	Kahramanmaraş	Elbistan	38.089	37.239	7.6	7.0
551067	20 February 2023, 20:04	Hatay	Yayladağı	36.037	36.021	6.4	21.73

A2. *Characteristics of recorded ground motions*

A fundamental technique for evaluating the frequency content of ground motion is Fourier analysis, which decomposes a periodic signal into a series of harmonic components with varying frequencies, amplitudes, and phases. The Fourier transform of a signal, typically the acceleration time-history a(t), is defined as shown in Eq. A1, where t denotes time and f denotes frequency. This approach is particularly effective for stationary signals – those whose frequency characteristics remain constant throughout the time series. However, its principal limitation lies in its inability to localise frequency components in time, thereby rendering it insufficient for the analysis of non-stationary signals, where the frequency content evolves over time (Fan, Zhu, and Zhang 2025).

$$A(f) = \int_{-\infty}^{\infty} a(t) \mathrm{e}^{-i2\pi f\tau} dt \tag{A1}$$

To address this limitation, time-frequency analysis techniques have been developed to characterise signals with temporal variations in spectral content. Among the more recent and promising methods is the Stockwell transform (also known as the S-transform) (Stockwell, Mansinha, and Lowe 1996), which is employed in this study to investigate the time-frequency characteristics of acceleration data from a high-order nonlinear system. Previous studies have established that the S-transform offers a reliable and computationally efficient alternative to the conventional Fast Fourier Transform (FFT) for seismic signal analysis (Asgari, Ranjbar, and Bagheri 2025; Pan et al. 2023). The S-transform allows for the assessment of how acceleration varies across different frequency bands during a seismic event, delivering improved temporal resolution relative to the short-time Fourier transform (STFT) and superior frequency resolution compared to the wavelet scalogram (Asgari and Bagheripour 2010). A distinctive advantage of the S-transform over conventional wavelet techniques is its capacity to provide frequency-dependent resolution while maintaining a direct linkage to the Fourier spectrum, thereby preserving absolute phase information (Yılmaz 2025). Mathematically, the S-transform of a signal a(t)a(t)a(t) is formulated as a modified continuous wavelet transform, in which the analysing wavelet is augmented by a phase correction term, as shown in Eq. A2.

$$S(t,f) = \int_{-\infty}^{\infty} a(\tau) \frac{|f|}{\sqrt{2\pi}} \exp\left[-\frac{(t-\tau)^2 f^2}{2}\right] \exp[-2i\pi f\tau] d\tau \tag{A2}$$

The S-transform integrates conceptual elements from both the windowed Fourier transform and wavelet transform, producing a balanced representation in both time and frequency domains. The resulting S-transform spectrogram illustrates the Stockwell amplitude as a function of time and frequency, enabling a detailed visual interpretation of spectral content evolution. Importantly, the S-transform retains the absolute phase of the input signal – a characteristic inherited from the Fourier framework – while offering adaptive resolution properties: higher temporal resolution at high frequencies and enhanced spectral resolution at low frequencies. This feature makes the method particularly suitable for the analysis of non-stationary seismic signals, where the energy distribution varies dynamically over time. To enhance visual interpretability, the spectrograms generated using the S-transform are commonly normalised by dividing each spectral amplitude by the maximum amplitude at the corresponding time instant. In the resulting visualisation, spectral amplitudes are colour-coded, with deep blue representing a value of zero and deep red indicating a normalised amplitude of 1.0. This colour scale facilitates a clear and intuitive understanding of how energy is distributed across time and frequency throughout the seismic record.

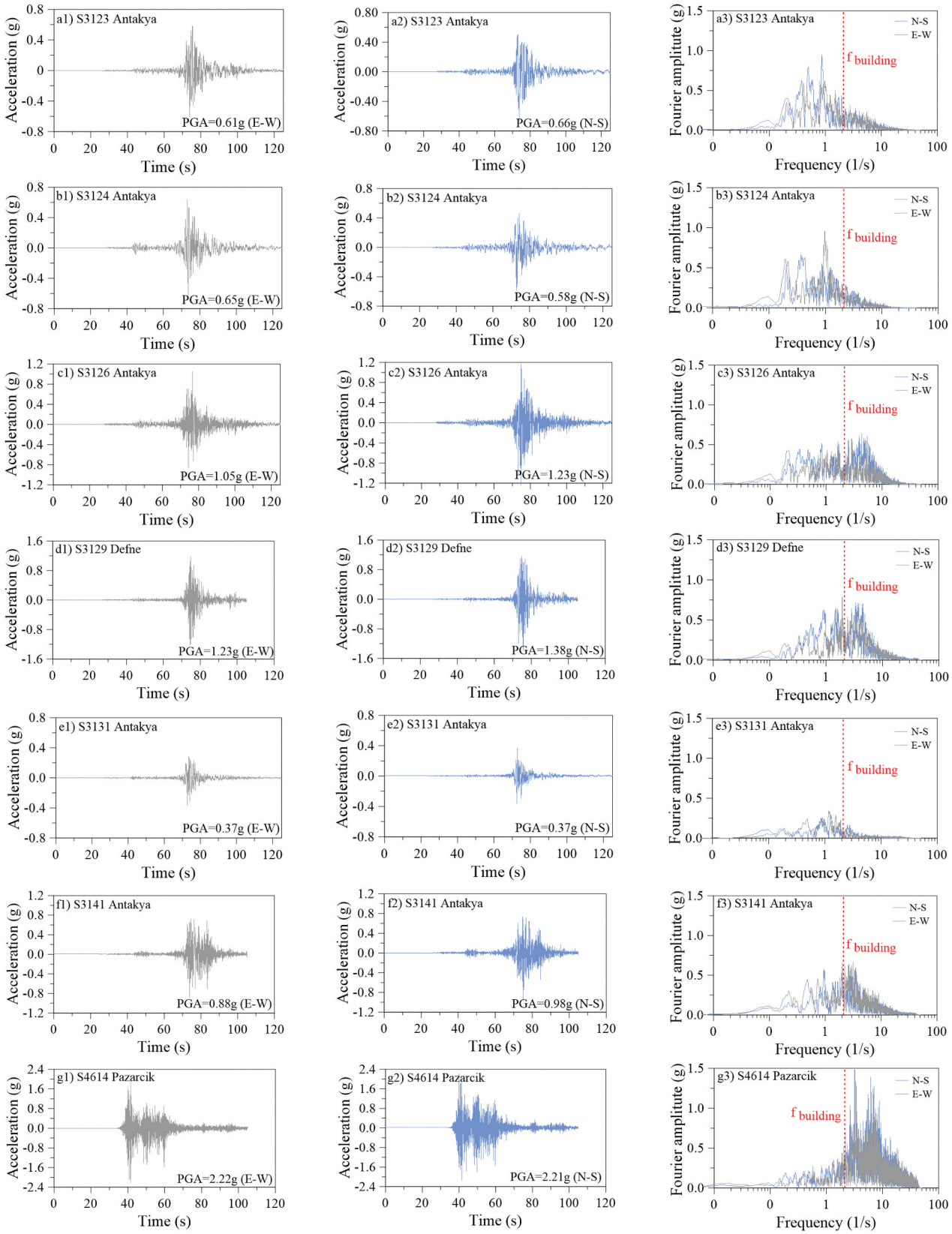

Figure A1. Selected ground motions of (a1-g1) *x* direction, (a2-g2) *y* direction, (a3-g3) Fourier Amplitude Spectra in both directions. "S" in S3123 refers to station.

Figure A1 shows the acceleration time histories for the *x* and *y* directions of the seven stations (S3123, S3124, S3126, S3131, S3141, S3129, and S4614), including peak values. Likewise, Figure A1 also shows the corresponding FAS amplitudes in both the N-S and E-W directions for such records. The red line in the FAS indicates the frequency of the case-study building. The smallest PGA and Fourier amplitude were found in S3131, while the largest was recorded at S4614, as shown in Fig A1. According to the Fourier plot of earthquake records, the period of the building generally falls outside the resonance zone. Figure A2 shows the spectral acceleration and velocity of the earthquake records (*x* and *y* directions) obtained from the stations (S3123, S3124,

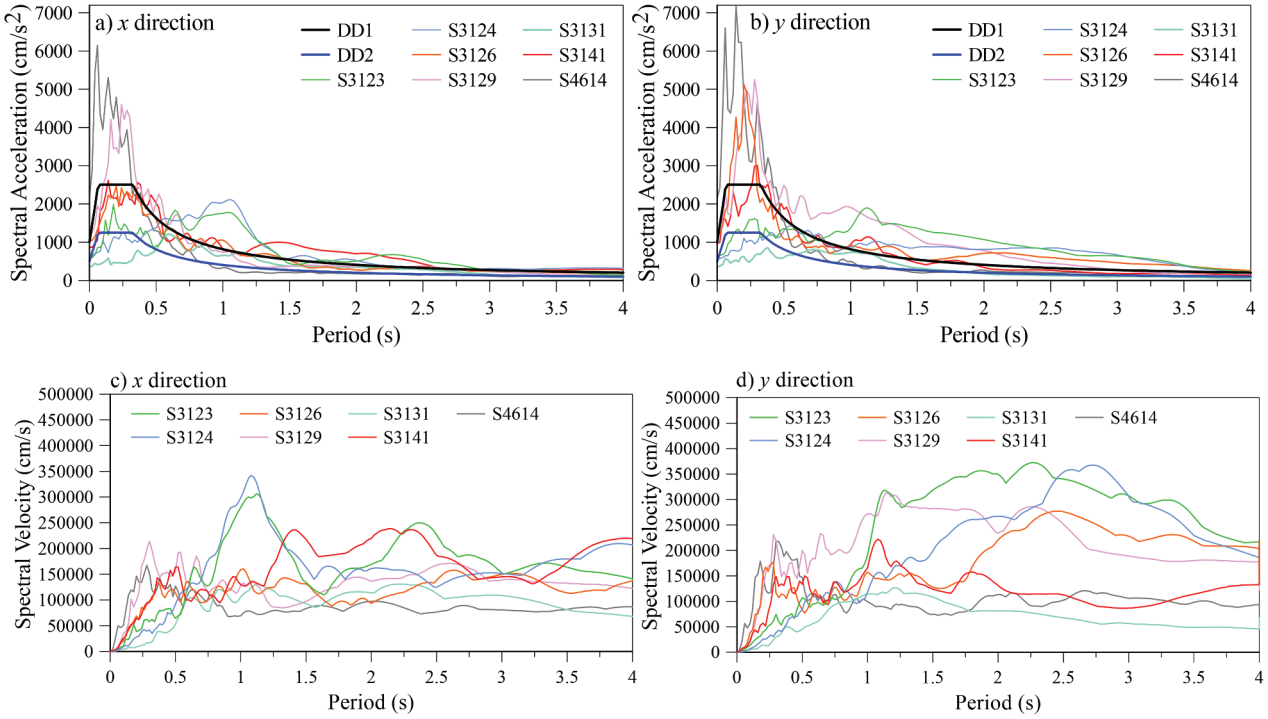

Figure A2. Horizontal response spectra (5% damping) vs TBEC 2018 spectrum in (a) *x* direction, (b) *y* direction, and spectral velocity in (c) *x* direction, (d) *y* direction for the selected stations.

S3126, S3129, S3131, S3141, and S4614), in addition to the earthquake ground motion level for the DD-1 and DD2 response spectra required by TBEC 2018.

Figure A3 presents the Stockwell transform spectrograms for three selected seismic stations: S3123, S3129, and S4614. Out of the seven available ground motion records, these three were chosen based on their representative seismic characteristics. Station S3123 is geographically closest to the structure under investigation, S3129 corresponds to the ground motion record that induced the highest dynamic response in the building, and S4614 recorded the peak ground acceleration (PGA) among all stations. As depicted in Figure A3a and A3b, for both S3123 and S3129, the Stockwell spectrograms reveal the signal amplitude at the structure's fundamental frequency of 2.12 Hz over the duration of seismic excitation (approximately from 20 to 100 seconds). Notably, the Stockwell amplitude observed in S3129 is consistently higher than that of S3123 along this frequency band. This is attributed to the relatively higher PGA and elevated frequency components present in the S3129 record. The higher spectral amplitude at the building's natural frequency supports the observed increase in the inter-story drift ratio when the structure is subjected to the S3129 input, as compared to S3123. Conversely, although S4614 recorded the highest PGA, it resulted in the smallest inter-story drift ratio. This counterintuitive response can be explained by examining the phase alignment between the ground motion and the structural frequency. As shown in Figure A3c, the 2.12 Hz frequency band (indicated by the black dashed line) exhibits minimal amplitude throughout the time-history, remaining in the deep blue range of the spectrogram. This indicates a lack of significant energy content at the building's resonant frequency, implying that the excitation was largely out of phase with the structural response. As a result, the ground motion from S4614, despite its high PGA, was less effective in exciting the building's dominant dynamic model.

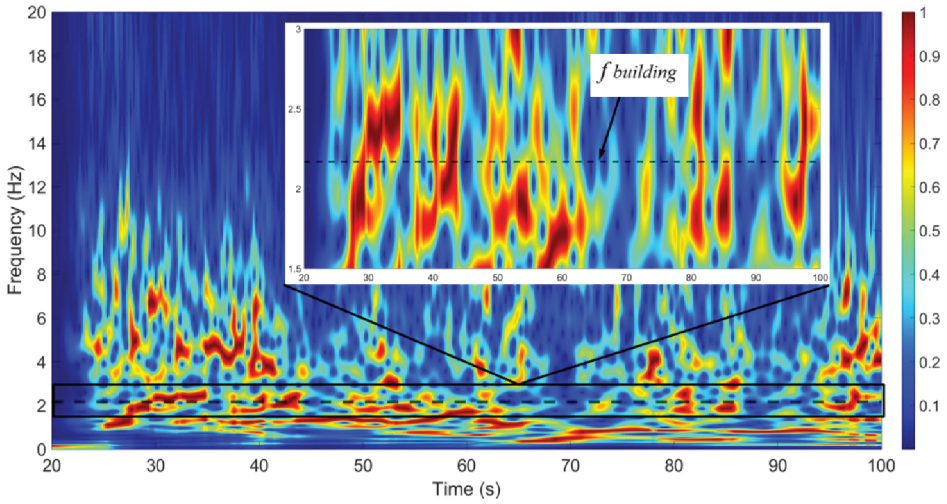

(a) S3123 Antakya (N-S)

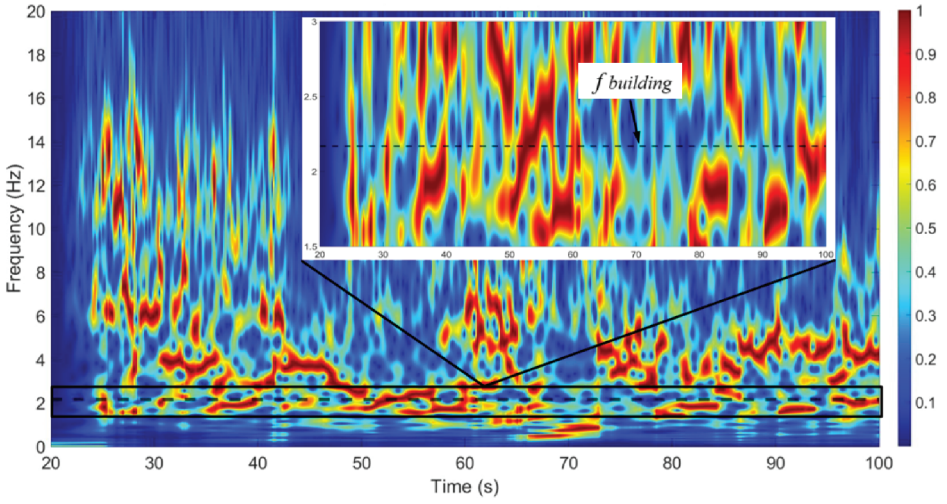

(b) S3129 Defne (N-S)

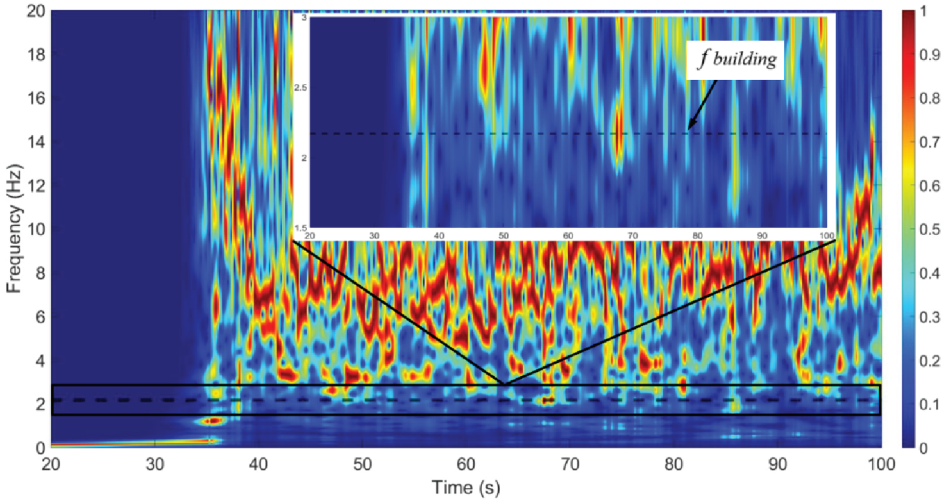

(c) S4614 Pazarcık (N-S)

Figure A3. Stockwell transform of the N – S components of stations S3123, S3129, and S4614.